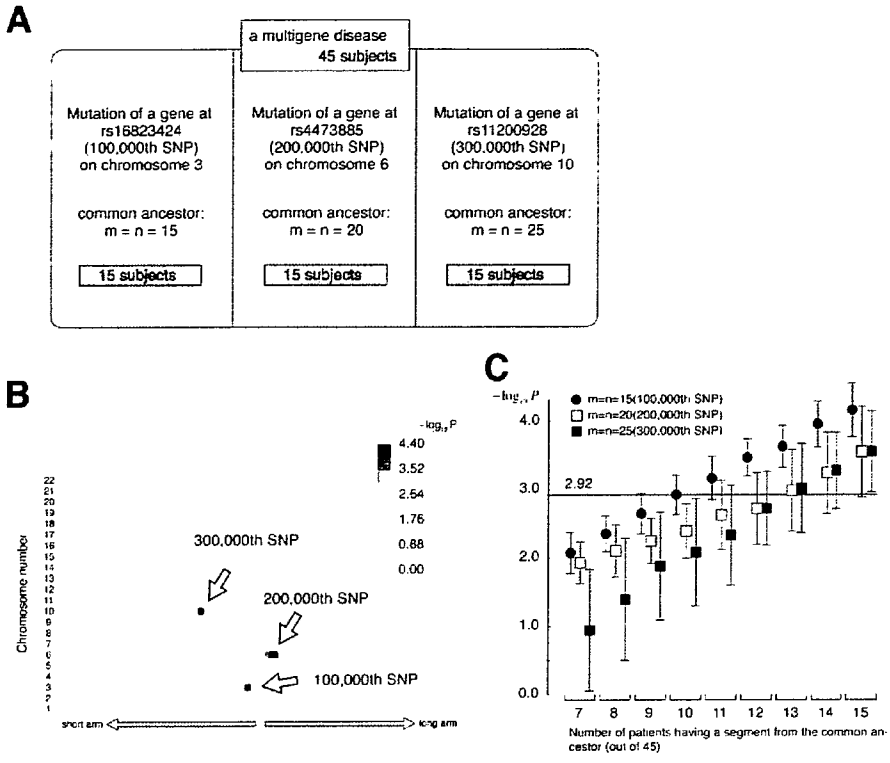

Figure 7. Multiple targets and the effect of the numbers of generations. *A*, Structure of the disease. *B*, An example of simultaneous detection of three regions. White arrows indicate the position of individual SNPs. A 2.56-cM-length region containing 100,000th SNP on chromosome 3, a 0.94-cM-length region containing the 200,000th SNP on chromosome 6 and a 2.55-cM-length containing the 300,000th SNP on chromosome 10 present the greatest $-\log_{10}(P)$ values in their neighborhood, and the values were 4.09, 4.39, and 3.49, respectively. *C*, The distribution of $-\log_{10}(P)$ from the analyses using 100 patient pools. The graph is similar to fig. 6*F*, and the data for three targets (100,000th SNP, 200,000th SNP, and 300,000th SNP) are simultaneously shown. The highest background value is 2.92.

crossover interference.[14] However, the crossover interference suppresses the production of short RCAs and favors the RCHHs in detecting true RCAs, so we made no adjustments for crossover interference in our calculation. For more-detailed discussion, see appendix A. If inbreeding exists in the pedigree, the segments from the common ancestor may be located on both copies of homologous autosomes, as in subject 2 in fig. 2*A*. This increases the average size of the RCAs and reduces the false negative rates. However, the rate of false positives may rise. The detailed information on inbreeding that occurred in previous generations is most often unknown. The practical approach to handling this is to calculate the false positives by use of the actual genotyping data, as illustrated in figure 6*D*, and to determine the RCHH cutoff. This compensates for the lack of information on inbreeding.

The numbers of SNPs used in this study were not sufficient to detect ancestral segments with an age of $m + n > 30$ (fig. 6*D*). The number of type A false positives is reduced as the number of SNPs increases (fig. 8). (The rate of type B false positives is heavily dependent on the actual genotyping data and thus was not plotted.) A larger number of SNPs will allow us to use a smaller RCHH cutoff. Figure 8 suggests that the genotyping data of 1,000,000 SNPs may expand the range of analysis to $m + n > 60$.

In the model multigene diseases, we used the patient pool containing 45 subjects. However, smaller numbers of subjects worked fine as well. For example, a pool of 18 subjects containing 6 subjects sharing an RCA clearly provided sufficient signal, although with a higher background (data not shown).

The four major methods for the identification of disease genes are the haplotype analysis, the linkage analysis, the sib-pair analysis and the whole-genome association studies.[15] The former two methods target single-gene diseases occurring in families (usually $m + n < 6$), whereas the latter two methods target both single-gene and multigene diseases occurring in the general population. When $m + n < 3$, HH analysis does not work well. In fact, the HH cannot distinguish parents from children, as shown in figure 5*A*, whereas haplotype analysis or linkage analysis may be able to identify a disease gene from pedigrees com-

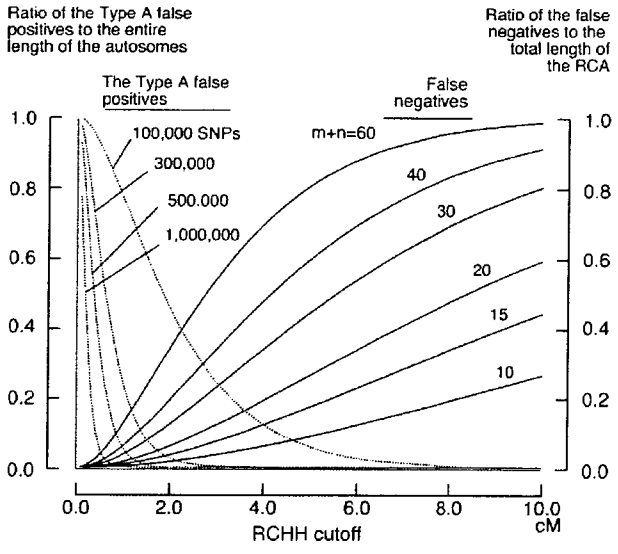

Figure 8. The effect of the numbers of SNPs used and the target generations of the analysis. The type A false positives were plotted for a range of numbers of the SNPs genotyped. The false negatives were plotted for a range of $m + n$ values.

posed of only two generations.[16] For families containing subjects with $m + n \geq 3$, HH analysis works well, as shown in figure 5. HH analysis may provide an advantage when $6 \leq m + n \leq 50$ where the haplotype analysis or the linkage analysis are difficult to perform. HH analysis is considered applicable to sib-pair analysis, where one sib pair provides 3/4 of the entire autosomes as shared regions (see eq. [1]). One attractive application may be for affected-relative-pair analyses.[17] Equation (1) indicates that one second-cousin pair may narrow the candidate autosomal region to 1/16 of the entire length of the autosomes, and three second-cousin pairs may narrow it further to $(1/16)^3 = 1/4{,}096$.

The simulation results presented in this study suggest that HH analysis demonstrates advantages and may complement whole-genome association studies by detecting genes for common diseases in the following situations. (1) The target population is genetically isolated. (2) The relative risk of the disease gene is moderate to high, and thus the frequencies of the disease-associated HH are expected to be significantly different between the patient pool and the control pool. (3) The common ancestors who brought the disease gene into the population are assumed to have existed within the last several hundred years, thus enabling the detection of the RCAs as RCHHs. (4) The number of the common ancestors who brought the disease gene was small, which limits the number of the disease-associated HHs in the population, and thus the frequencies of some of them may exceed the detection limit shown in figures 6*F* and 7*C*. When these conditions are met, the inclusion of only a few dozen patients may be required to identify the location of the disease gene (figs. 6 and 7). However, the identified regions may be 1–3 cM in length and require more-detailed investigation. Ethnically, geographically, or culturally isolated populations may fulfill these requirements for many diseases. For example, consider the French-Canadian population in Quebec.[18,19] It is known that two-thirds of the genetic pool of the current population of 6 million people is derived from only 2,600 settlers who arrived during the 17th century (i.e., $m = n = 20$, given 20 years per generation). The causative genes for diseases with an incidence of ≤ 0.01 may be derived from only one or two dozen common ancestors. In other words, the number of the disease-associated HH was limited to one or two dozen because of the bottleneck effect caused by the immigration. If random genetic drift is taken into consideration, some of the disease-associated HH may exceed the detection limit of 29% in the patient pool (fig. 7*B*). Therefore, moderate- to high-risk genes for diseases with an incidence of ≤ 0.01 in Quebec fulfills all four requirements and is therefore worth studying by HH analysis, whether the gene is for a single-gene disease or a multigene disease. If any one of the four conditions is not met, HH analysis should not be considered a good choice. The selection of the target population and the target disease are crucial.

In this study, we describe the introduction of the HH and its applications. The HH is easy to obtain and the results are intuitive. Although modern society promotes the movement of people, many countries have a history in which the transfer of people was politically or geographically limited. Patients with a specific disease clustered in a geographical region therefore may inherit a common ancestral disease gene. In such regions, HH analysis may provide a distinct benefit. We believe that HH analysis will therefore facilitate the identification of disease genes both for single-gene and multigene diseases.

Acknowledgments

We thank Prof. Hideshi Kawakami, Hiroshima University, Japan, for his critical review of the manuscript, and Ms. Yukiko Yatsuka, for her valuable technical assistance. This work was supported in part by the following grants-in-aid: (1) for scientific research (No. 18390242) from the Japan Society for the Promotion of Science, (2) for Comprehensive Research on Aging and Health from the Ministry of Health, Labor, and Welfare, Japan, and (3) from the Ministry of Education, Culture, Sports, Science, and Technology of Japan, in particular by a Ministry Grant to the Saitama Medical University Research Center for Genomic Medicine.

Appendix A

Deduction of Equation (1)

The calculation to obtain RCA(1,1) is presented as an example (fig. A1). A and B are the common ancestors. m1–

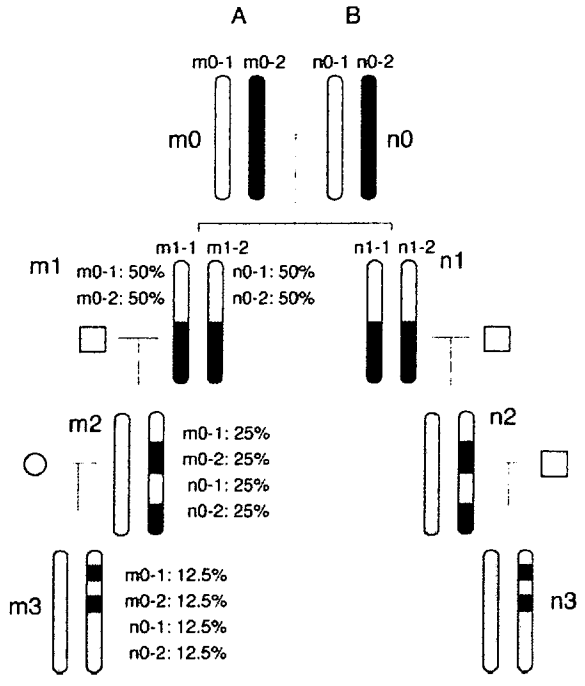

Figure A1. Deduction of equation (1). Gray circles and boxes indicate spouses. Gray areas of the chromosomes come from spouses and do not contain segments from the common ancestors (i.e., A and B).

1 and m1–2 are two copies of homologous chromosomes for subject m1, and n1–1 and n1–2 are two copies of homologous chromosomes for subject n1. One half of m1–1 is from m0–1, and the other half is from m0–2. One half of n1–1 is from n0–1, and the other half is from n0–2. Between subjects m1 and n1, the ratio of the RCA to the entire chromosome is calculated as the probability that m1 and n1 share the same chromosomal segment at a specific position on chromosomes. It can be obtained by subtracting from 1 the probability that m1–1, m1–2, n1–1, and n1–2 all have segments derived from different chromosomes. Therefore,

$$\mathrm{RCA}(1,1) = 1 - \frac{1}{2} \times \frac{1}{2} = \frac{3}{4} .$$

RCA(m,n) for other values of m and n were similarly obtained and summarized in equation (1).

Calculation of False Negatives, Type A False Positives, and Type B False Positives

Step 1: Ratio of False Negatives to Total Length of RCAs ($R_{\text{false negatives}}$).—According to the Haldane's Poisson model, the length (x, in centimorgans) of the chromosomal segment derived from an ancestral chromosome in generation m (see fig. 2*B*) has an exponential distribution that has the probability density function

$$f(x) = \lambda e^{-\lambda x} ,$$
$$\lambda = \frac{m}{100} . \qquad \text{(A1)}$$

First, the union of ancestral chromosomal segments on two homologous chromosomes are taken for each subject. Next, the RCAs are the intersections of these unions between the two subjects. From equation A1, when $m + n$ (see fig. 2*B*) is large enough, $R_{\text{False negatives}}$ for an RCHH cutoff c is approximated by

$$R_{\text{False negatives}} \approx \frac{\int_0^c x f(x) dx}{\int_0^\infty x f(x) dx}$$
$$= 1 - e^{-\lambda c}(1 + \lambda c) , \qquad \text{(A2)}$$

where

$$f(x) = \lambda e^{-\lambda x}$$
$$\lambda = \frac{m+n}{100} .$$

However, when $m + n$ is small, the $R_{\text{False negatives}}$ deviates from the value calculated by equation (A2). We therefore obtained $R_{\text{False negatives}}$ for small values of $m + n$ by the Monte Carlo method, with use of 100,000 pedigrees (table A1). We found that equation (A2) provides good approximations when $m + n > 12$ (see table A1; compare the values for $m + n = 12$).

Step 2: Ratio of the Type A False Positives to the Entire Autosome ($R_{\text{Type A false positives}}$).—Given that N_{SNP} is the total number of SNPs on a genotyping chip, and P_n and Q_n are the frequencies of the major and minor alleles for the nth SNP, respectively, the average frequencies of the major alleles ($\bar{F}_{\text{major allele}}$) and the minor alleles ($\bar{F}_{\text{minor allele}}$) are

$$\bar{F}_{\text{major allele}} = \frac{\sum_{n=1}^{N_{\text{SNP}}} P_n}{N_{\text{SNP}}}$$

and

$$\bar{F}_{\text{minor allele}} = \frac{\sum_{n=1}^{N_{\text{SNP}}} Q_n}{N_{\text{SNP}}} ,$$

respectively. The number of mismatched compSNPs ($N_{\text{mismatched compSNP}}$) is approximated by

$$N_{\text{mismatched compSNP}} \approx \frac{2\left(\bar{F}_{\text{major allele}}\right)^2\left(\bar{F}_{\text{minor allele}}\right)^2 N_{Pt1}N_{Pt2}}{N_{SNP}},$$

where N_{Pt1} and N_{Pt2} are the numbers of SNPs successfully genotyped for Pt1 and Pt2, respectively. $N_{\text{mismatched compSNP}}$ is not a large number. For example, with use of the 500k GeneChips from Affymetrix, $N_{\text{mismatched compSNP}}$ is 22,000 at maximum, spaced at 0.16 cM on average. This spacing is larger in size than most of the haplotype blocks and thus is assumed to be randomly distributed over the entire autosome. The length between two mismatched compSNPs is considered to have an exponential distribution with a density probability function of

$$f(x) = \lambda e^{-\lambda x},$$

$$\lambda = \frac{N_{\text{mismatched compSNP}}}{L_{\text{autosome}}},$$

where L_{autosome} is the entire genetic length of the autosomes. Therefore, for the cutoff value c,

$$R_{\text{Type A false positives}} = \frac{\int_c^\infty xf(x)dx}{\int_0^\infty xf(x)dx} = (1 + \lambda c)e^{-\lambda c}.$$

Step 3: Ratio of the Type B False Positives to the Entire Length of the Autosomes ($R_{\text{Type B false positives}}$).—An RCHH containing an RCA is expected to have the type B false positives with a length of $\frac{\text{cut off value}}{2}$ on each end. It is impossible to distinguish RCHHs that contain the RCAs from those that do not (i.e., the type A false positives). We calculated $R_{\text{Type B false positives}}$ under the assumption that every RCHH contains an RCA. Therefore, the $R_{\text{Type B false positives}}$ calculation results in an overestimation, which we consider to be more appropriate than an underestimation when the appropriate RCHH cutoff is being determined.

The Representative

The easiest way to compare the patient pool and the control pool is to directly compare the number of patients sharing the RCHHs at the given position (fig. A2*A*). This algorithm usually works fine, but actually this reduces the sensitivity. Assume that, at a specific position, the patient pool has 4 subjects sharing HH1 and has 0 subject sharing HH2. The control pool has 0 subject sharing HH1 and 4 subjects sharing HH2. Although two pools are different in their frequency of HH1, the algorithm shown in figure A2*A* does not detect it.

One of the ways to solve this problem is to have a representative, as shown in fig. A2*B*, as we did in this study. For the actual algorithm, please see the program source code. This algorithm may have difficulty picking up the most common HHs in a region where there is no dominant HH but only many kinds of HHs with low frequencies, which we think does not cause any major problems. We have also provided the source code for an alternative algorithm. The source may be modified according to your uses.

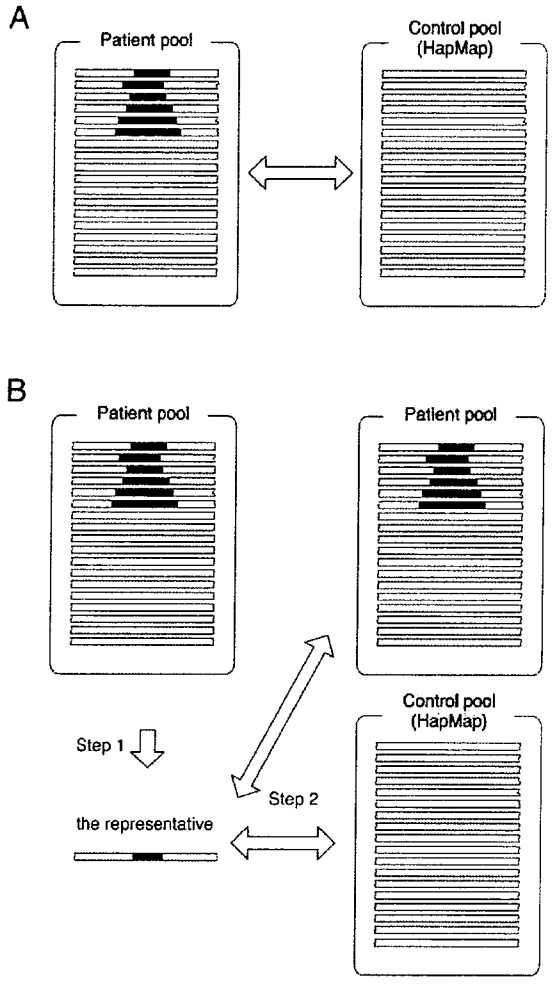

Figure A2. Two strategies for comparing the patient pool with the control pool.

Crossover Interference and the Size of the RCAs

Crossover interference increases the average size of the RCA, and favors the RCHHs in detecting the RCA, which reduces the false negatives. This results in a better performance in HH analysis. Figure A3 shows an RCA in one generation. The size of RCA may be reduced in size in the next generation. The reduction occurs by two processes: (1) crossover occurs in one or both subjects and (2) mul-

Table A1. Ratios of False Negatives to the Total Length of the RCAs for a Range of RCHH Cutoffs

Calculation Method and Variable(s)			Ratio of False Negatives to Total Length of the RCAs, by RCHH Cutoff (in cM)																													
			.2	.4	.6	.8	1	1.2	1.4	1.6	1.8	2	2.2	2.4	2.6	2.8	3	3.2	3.4	3.6	3.8	4	4.2	4.4	4.6	4.8	5	5.2	5.4	5.6	5.8	6
Monte Carlo																																
$m+n$	m	n																														
2	2	0	.000	.000	.000	.000	.000	.000	.000	.000	.000	.001	.001	.001	.001	.001	.001	.001	.002	.002	.002	.002	.003	.003	.003	.003	.004	.004	.004	.004	.005	.005
	1	1	.000	.000	.000	.000	.000	.000	.001	.001	.001	.001	.001	.001	.002	.002	.002	.003	.003	.003	.004	.004	.004	.005	.005	.005	.006	.006	.007	.007	.008	.008
3	3	0	.000	.000	.000	.000	.000	.001	.001	.001	.001	.002	.002	.002	.003	.003	.003	.004	.004	.005	.005	.006	.007	.007	.008	.008	.009	.010	.011	.012	.012	.013
	2	1	.000	.000	.000	.000	.001	.001	.001	.001	.002	.002	.003	.003	.004	.004	.005	.005	.006	.007	.008	.008	.009	.010	.011	.012	.013	.014	.015	.016	.017	.018
4	4	0	.000	.000	.000	.000	.001	.001	.001	.002	.002	.003	.003	.004	.005	.005	.006	.007	.008	.009	.010	.011	.012	.013	.014	.015	.017	.018	.019	.021	.022	.024
	3	1	.000	.000	.000	.001	.001	.001	.002	.002	.003	.004	.004	.005	.006	.007	.008	.009	.010	.011	.013	.014	.015	.017	.018	.019	.021	.022	.024	.026	.028	.029
	2	2	.000	.000	.000	.001	.001	.002	.002	.003	.004	.004	.005	.006	.007	.009	.010	.011	.013	.014	.015	.017	.019	.020	.022	.024	.026	.028	.030	.032	.034	.036
5	5	0	.000	.000	.000	.001	.001	.002	.002	.003	.004	.004	.005	.006	.007	.008	.010	.011	.012	.014	.015	.017	.019	.020	.022	.024	.026	.028	.030	.032	.034	.037
	4	1	.000	.000	.001	.001	.001	.002	.003	.004	.004	.005	.007	.008	.009	.010	.012	.013	.015	.017	.019	.020	.022	.025	.027	.029	.031	.034	.036	.039	.041	.044
	3	2	.000	.000	.001	.001	.002	.002	.003	.004	.005	.006	.008	.009	.011	.012	.014	.016	.018	.020	.022	.024	.026	.029	.031	.034	.036	.039	.042	.044	.047	.050
6	6	0	.000	.000	.001	.001	.002	.002	.003	.004	.005	.006	.008	.009	.010	.012	.014	.016	.018	.020	.022	.024	.026	.029	.031	.034	.036	.039	.041	.044	.047	.050
	5	1	.000	.000	.001	.001	.002	.003	.004	.005	.006	.007	.009	.011	.013	.014	.016	.018	.020	.023	.025	.028	.030	.033	.036	.039	.042	.045	.049	.052	.056	.059
	4	2	.000	.000	.001	.001	.002	.003	.004	.006	.007	.009	.010	.012	.014	.016	.018	.021	.023	.026	.029	.032	.035	.038	.041	.044	.048	.051	.055	.059	.062	.066
	3	3	.000	.000	.001	.001	.002	.003	.004	.006	.007	.009	.010	.012	.014	.016	.019	.021	.024	.026	.029	.032	.035	.038	.042	.045	.048	.052	.055	.059	.063	.066
7	6	1	.000	.000	.001	.002	.003	.004	.005	.006	.008	.010	.011	.013	.016	.018	.021	.023	.026	.029	.033	.036	.040	.043	.046	.050	.054	.058	.063	.067	.071	.075
	5	2	.000	.000	.001	.002	.003	.004	.006	.007	.009	.011	.013	.016	.018	.021	.024	.027	.030	.034	.037	.041	.044	.048	.052	.056	.061	.065	.070	.075	.080	.084
	4	3	.000	.000	.001	.002	.003	.004	.006	.007	.009	.011	.013	.016	.018	.021	.024	.026	.030	.033	.037	.040	.044	.048	.052	.056	.061	.065	.069	.074	.078	.083
8	6	2	.000	.001	.001	.003	.004	.005	.007	.009	.012	.014	.017	.020	.023	.026	.029	.033	.037	.041	.046	.050	.055	.060	.064	.069	.075	.081	.086	.092	.097	.103
	5	3	.000	.001	.001	.002	.004	.005	.007	.009	.011	.014	.017	.019	.022	.026	.029	.032	.036	.040	.045	.050	.054	.059	.063	.069	.074	.080	.085	.091	.096	.101
	4	4	.000	.001	.001	.002	.004	.005	.007	.009	.011	.014	.017	.019	.022	.026	.029	.032	.036	.040	.045	.049	.054	.059	.063	.068	.073	.079	.084	.089	.094	.099
9	6	3	.000	.001	.002	.003	.005	.007	.009	.012	.015	.017	.020	.024	.027	.031	.035	.039	.044	.049	.055	.061	.067	.073	.079	.085	.092	.098	.104	.111	.117	.124
	5	4	.000	.001	.002	.003	.004	.006	.009	.011	.013	.016	.019	.022	.026	.030	.034	.038	.043	.047	.052	.057	.063	.069	.074	.081	.088	.094	.100	.105	.111	.118
10	6	4	.000	.001	.002	.004	.006	.008	.011	.014	.017	.021	.024	.028	.032	.036	.041	.046	.051	.056	.062	.068	.074	.081	.090	.097	.104	.111	.119	.126	.134	.142
	5	5	.000	.001	.002	.003	.005	.007	.011	.014	.016	.019	.023	.027	.031	.035	.040	.045	.051	.056	.062	.068	.074	.081	.088	.095	.102	.110	.117	.124	.131	.138
11	6	5	.000	.001	.002	.004	.007	.009	.013	.016	.019	.023	.027	.032	.037	.042	.047	.053	.060	.066	.072	.080	.089	.096	.103	.110	.117	.125	.133	.141	.150	.158
12	6	6	.000	.001	.003	.005	.008	.010	.014	.019	.023	.027	.032	.037	.042	.049	.056	.063	.069	.077	.084	.092	.101	.111	.120	.128	.137	.145	.152	.159	.166	.173
Eq. (A1)																																
$m+n$	m	n																														
12			.000	.001	.002	.004	.007	.009	.013	.016	.020	.025	.029	.034	.040	.045	.051	.057	.064	.070	.077	.084	.091	.099	.106	.114	.122	.130	.138	.146	.154	.163
13			.000	.001	.003	.005	.008	.011	.015	.019	.023	.028	.034	.040	.046	.052	.059	.066	.073	.081	.088	.096	.104	.113	.121	.130	.139	.148	.157	.166	.175	.184
14			.000	.002	.003	.006	.009	.013	.017	.022	.027	.033	.039	.045	.052	.059	.067	.075	.083	.091	.100	.109	.118	.127	.137	.146	.156	.166	.175	.185	.196	.206
15			.000	.002	.004	.007	.010	.014	.019	.025	.031	.037	.044	.051	.059	.067	.075	.084	.093	.103	.112	.122	.132	.142	.152	.163	.173	.184	.195	.206	.217	.228
16			.000	.002	.004	.008	.012	.016	.022	.028	.034	.041	.049	.057	.066	.075	.084	.094	.104	.114	.125	.135	.146	.157	.168	.180	.191	.203	.214	.226	.238	.250
17			.001	.002	.005	.008	.013	.018	.024	.031	.038	.046	.055	.064	.073	.083	.093	.104	.115	.126	.137	.149	.161	.173	.185	.197	.209	.222	.234	.247	.259	.272
18			.001	.002	.005	.009	.014	.020	.027	.034	.042	.051	.060	.070	.081	.091	.103	.114	.126	.138	.150	.163	.175	.188	.201	.214	.228	.241	.254	.267	.280	.294
19			.001	.003	.006	.010	.016	.022	.030	.038	.047	.056	.066	.077	.088	.100	.112	.125	.137	.150	.163	.177	.190	.204	.218	.232	.246	.260	.274	.288	.302	.316
20			.001	.003	.007	.012	.018	.025	.033	.041	.051	.062	.073	.084	.096	.109	.122	.135	.149	.163	.177	.191	.206	.220	.235	.250	.264	.279	.294	.308	.323	.337
25			.001	.005	.010	.018	.027	.037	.049	.062	.075	.090	.106	.122	.139	.156	.173	.191	.209	.228	.246	.264	.283	.301	.319	.337	.355	.373	.391	.408	.425	.442
30			.002	.007	.014	.025	.037	.051	.067	.084	.103	.122	.142	.163	.184	.206	.228	.250	.272	.294	.316	.337	.359	.380	.401	.422	.442	.462	.482	.501	.519	.537
35			.002	.009	.019	.033	.049	.067	.087	.109	.132	.156	.180	.206	.231	.257	.283	.308	.334	.359	.384	.408	.432	.455	.478	.501	.522	.543	.563	.583	.602	.620
40			.003	.012	.025	.041	.062	.084	.109	.135	.163	.191	.220	.250	.279	.308	.337	.366	.394	.422	.449	.475	.501	.525	.549	.572	.594	.615	.636	.655	.674	.692
50			.005	.018	.037	.062	.090	.122	.156	.191	.228	.264	.301	.337	.373	.408	.442	.475	.507	.537	.566	.594	.620	.645	.669	.692	.713	.733	.751	.769	.785	.801
60			.007	.025	.051	.084	.122	.163	.206	.250	.294	.337	.380	.422	.462	.501	.537	.572	.605	.636	.665	.692	.717	.740	.762	.782	.801	.818	.834	.849	.862	.874

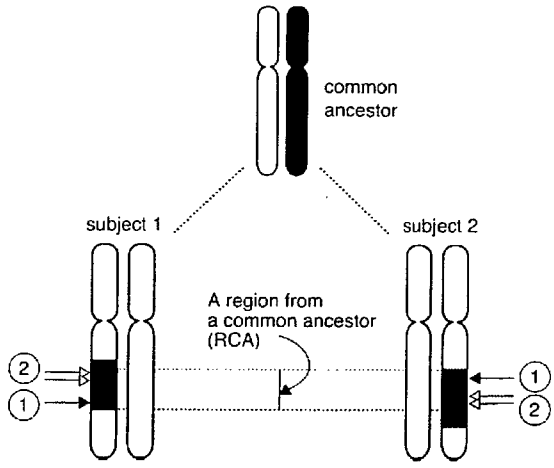

Figure A3. Effects of crossover interference. Process numbers are enclosed in the circle. Processes 1 and 2 both reduce the length of the RCAs in the next generation. Process 1 is independent of and process 2 is dependent on the crossover interference. *Gray area,* shared segments derived from a common ancestor.

tiple crossovers occur in one or both subjects. Although occurrence of process 2 may be suppressed by crossover interference, process 1 is independent of the interference and is not suppressed. Moreover, as the size of the shared segments from the common ancestor (shown in gray in fig. A3) shortens over generations, multiple crossovers in a single RCA become less frequent, even without crossover interference, and process 1 becomes the main determinant of the size of the RCAs. Therefore, crossover interference has a limited effect on HH analysis, and so we chose not to make any adjustment in the algorithm.

Web Resources

URLs for data presented herein are as follows:

Affymetrix, http://www.affymetrix.com/index.affx
GCC, the GNU Compiler Collection, http://gcc.gnu.org/
K.H.'s Web site, http://homepage.mac.com/hagiwark/FileSharing1.html (for HH analysis program)
International HapMap Project, http://www.hapmap.org/
National Center for Biotechnology Information, http://www.ncbi.nlm.nih.gov/
Online Mendelian Inheritance in Man (OMIM), http://www.ncbi.nlm.nih.gov/Omim/
Saitama Medical University, http://www.saitama-med.ac.jp/genome/TR/hh_analysis_program_and_manual.zip (for HH analysis program and manual)

References

1. Long JC, Williams RC, Urbanek M (1995) An E-M algorithm and testing strategy for multiple-locus haplotypes. Am J Hum Genet 56:799–810
2. Morton NE (1955) Sequential tests for the detection of linkage. Am J Hum Genet 7:277–318
3. Kruglyak L, Lander ES (1995) Complete multipoint sib-pair analysis of qualitative and quantitative traits. Am J Hum Genet 57:439–454
4. International HapMap Consortium (2003) The International HapMap Project. Nature 426:789–796
5. Di Rienzo A, Hudson RR (2005) An evolutionary framework for common diseases: the ancestral-susceptibility model. Trends Genet 21:596–601
6. Carlson CS, Eberle MA, Kruglyak L, Nickerson DA (2004) Mapping complex disease loci in whole-genome association studies. Nature 429:446–452
7. Gillanders EM, Pearson JV, Sorant JM, Trent JM, O'Connell JR, Bailey-Wilson JE (2006) The value of molecular haplotypes in a family-based linkage study. Am J Hum Genet 79:458–468
8. Amos CI, Dawson DV, Elston RC (1990) The probabilistic determination of identity-by-descent sharing for pairs of relatives from pedigrees. Am J Hum Genet 47:842–853
9. Zhang K, Zhao H (2006) A comparison of several methods for haplotype frequency estimation and haplotype reconstruction for tightly linked markers from general pedigrees. Genet Epidemiol 30:423–437
10. Haldane JBS (1919) The combination of linkage values, and the calculation of distances between the loci of linked factors. J Genet 8:299–309
11. Kong A, Gudbjartsson DF, Sainz J, Jonsdottir GM, Gudjonsson SA, Richardsson B, Sigurdardottir S, Barnard J, Hallbeck B, Masson G, et al (2002) A high-resolution recombination map of the human genome. Nat Genet 31:241–247
12. Hayward C, Brock DJ (1997) Fibrillin-1 mutations in Marfan syndrome and other type-1 fibrillinopathies. Hum Mutat 10:415–423
13. Pritchard DJ, Korf BR (2003) Medical genetics at a glance. Blackwell Publishing, Birmingham, United Kingdom
14. Sturtevant AH (1915) The behavior of chromosomes as studied through linkage. Z Indukt Abstammungs-Vererbungsl 13:234–287
15. Strachan T, Read A (2003) Human molecular genetics. Garland Science/Taylor & Francis Group, Oxfordshire, United Kingdom
16. Shore EM, Xu M, Feldman GJ, Fenstermacher DA, Brown MA, Kaplan FS (2006) A recurrent mutation in the BMP type I receptor ACVR1 causes inherited and sporadic fibrodysplasia ossificans progressiva. Nat Genet 38:525–527
17. Risch N (1990) Linkage strategies for genetically complex traits. II. The power of affected relative pairs. Am J Hum Genet 46:229–241
18. Heyer E, Tremblay M (1995) Variability of the genetic contribution of Quebec population founders associated to some deleterious genes. Am J Hum Genet 56:970–978
19. Laberge AM, Michaud J, Richter A, Lemyre E, Lambert M, Brais B, Mitchell GA (2005) Population history and its impact on medical genetics in Quebec. Clin Genet 68:287–301

Mutations in the *SLC34A2* Gene Are Associated with Pulmonary Alveolar Microlithiasis

Huqun, Shinyu Izumi, Hitoshi Miyazawa, Kuniaki Ishii, Bine Uchiyama, Tadashi Ishida, Sawako Tanaka, Ryushi Tazawa, Shunichiro Fukuyama, Tomoaki Tanaka, Yoshiaki Nagai, Akemi Yokote, Hiroki Takahashi, Toshihiko Fukushima, Kunihiko Kobayashi, Hirofumi Chiba, Makoto Nagata, Susumu Sakamoto, Koichiro Nakata, Yuji Takebayashi, Yoshihiko Shimizu, Koichi Kaneko, Michio Shimizu, Minoru Kanazawa, Shosaku Abe, Yoshikazu Inoue, Seiichi Takenoshita, Kunihiko Yoshimura, Koichiro Kudo, Teruo Tachibana, Toshihiro Nukiwa, and Koichi Hagiwara

Departments of Respiratory Medicine, Pathology, and Chest Surgery, Saitama Medical University, Saitama; Department of Respiratory Oncology and Molecular Medicine, Tohoku University, Sendai; Department of Pulmonary Medicine, Disease Control and Prevention Center, International Medical Center of Japan; Department of Respiratory Medicine, Tama Hokubu Hospital; Department of Respiratory Medicine, Respiratory Center, Toranomon Hospital, Tokyo; Department of Cardiovascular Pharmacology, Yamagata University, Yamagata; Department of Respiratory Medicine, Katta General Hospital, Miyagi; Department of Respiratory Medicine, Kurashiki Central Hospital, Okayama; Third Department of Internal Medicine, Sapporo Medical University, Sapporo; Department of Surgery II, Fukushima Medical University, Fukushima; Clinical Research Center, National Hospital Organization, Kinki-chuo Chest Medical Center; and Osaka Kampo Medical Center, Osaka, Japan

Rationale: Pulmonary alveolar microlithiasis is an autosomal recessive disorder in which microliths are formed in the alveolar space.
Objectives: To identify the responsible gene that causes pulmonary alveolar microlithiasis.
Methods: By means of a genomewide single-nucleotide polymorphism analysis using DNA from three patients, we have narrowed the region in which the candidate gene is located. From this region, we have identified a gene that has mutations in all patients with pulmonary alveolar microlithiasis.
Measurements and Main Results: We identified a candidate gene, *SLC34A2,* that encodes a type IIb sodium phosphate cotransporter and that is mutated in six of six patients investigated. *SLC34A2* is specifically expressed in type II alveolar cells, and the mutations abolished the normal gene function.
Conclusion: Mutations in the *SLC34A2* gene that abolish normal gene function cause pulmonary alveolar microlithiasis.

Keywords: pulmonary alveolar microlithiasis; homozygosity mapping; GeneChip; single-nucleotide polymorphisms

Pulmonary alveolar microlithiasis (PAM; OMIM [Online Mendelian Inheritance in Man] 265100) is a disease in which microliths are formed in the alveolar space (Figure 1A) (1–3). Ever since the first description by Puhr in 1933 (4), over 500 cases have been reported worldwide, including more than 100 cases in Japan (5). Patients remain symptom free until middle age when chronic respiratory failure and cardiopulmonary decompensation develop. In a chest X-ray image, diffuse fine nodular opacities formed by countless microliths are observed (Figure 1B). PAM has been considered to be an autosomal recessive disorder, because it transmits horizontally and inbreeding frequently coexists (3).

AT A GLANCE COMMENTARY

Scientific Knowledge on the Subject

Pulmonary alveolar microlithiasis is an autosomal recessive disorder in which microliths are formed in the alveolar space. However, the responsible gene has not been identified.

What This Study Adds to the Field

Mutation of the *SLC34A2* gene that encodes the sodium-dependent phosphate transporter causes pulmonary alveolar microlithiasis.

To identify the responsible gene for diseases with an autosomal recessive trait, the homozygosity mapping approach has been successfully applied (6). This method has identified the gene from fewer than 10 patients. Recent technological development has enabled high-density, genomewide single-nucleotide polymorphism (SNP) analysis. The numbers of SNPs genotyped are so great that fine mapping of the candidate region for the gene is anticipated. To efficiently use the SNP data, we have developed a novel algorithm based on the homozygosity mapping, and have used it to identify the gene responsible for PAM.

Preliminary (7–9) and final results of this study (10, 11) have been presented in the form of abstracts.

METHODS

Subjects and Ethical Considerations

The study was approved by the institutional review boards of the participating institutions. For all cases, written, informed consent was obtained from either the patient or from a family member.

Genotyping

We isolated genomic DNA either from blood samples or from paraffin-embedded tissues using standard protocols. For the whole-genome scan, we used the GeneChip Human Mapping 100k set (Affymetrix, Santa Clara, CA). The scan was performed at the Australian Genome Research Facility (Victoria, Australia) and AROS Applied Biotechnology (Aarhus Nord, Denmark). Computer analyses of the GeneChip results were performed using custom programs written in our laboratory (source codes available on request). The nucleotide sequencing of the

(Received in original form September 7, 2006; accepted in final form November 7, 2006)

Supported in part by the grant-in-aid for scientific research (No. 16659216) from the Japan Society for the Promotion of Science.

Correspondence and requests for reprints should be addressed to Koichi Hagiwara, M.D., Ph.D., Professor, Department of Respiratory Medicine, Saitama Medical University, 38 Morohongo, Moroyama-machi, Iruma-gun, Saitama 350-0495, Japan. E-mail: hagiwark@saitama-med.ac.jp

This article has an online supplement, which is accessible from this issue's table of contents at www.atsjournals.org

Am J Respir Crit Care Med Vol 175. pp 263–268, 2007
Originally Published in Press as DOI: 10.1164/rccm.200609-1274OC on November 9, 2006
Internet address: www.atsjournals.org

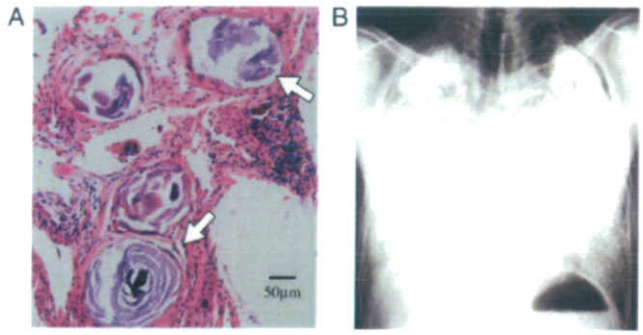

Figure 1. Microscopic and chest X-ray images of pulmonary alveolar microlithiasis (PAM). (*A*) A thin section of the decalcified lung tissue from patient 5 stained with hematoxylin and eosin. Concentric lamellar structures are decalcified remnants of microliths that occupied the entire alveolar space (*arrows*). Alveolar walls are thickened and many inflammatory cells have infiltrated into the parenchyma, indicating the presence of chronic inflammation. (*B*) A chest X-ray image of patient 2. Countless microliths form diffuse fine nodular opacities. The "snowstorm" appearance is very characteristic.

individual exons of *SLC34A2* was performed using an ABI 377 automated sequencer (Applied Biosystems, Foster City, CA).

Frequency of the Mutation of *SLC34A2* in the Japanese Population

Using a 5′ nuclease assay (for exon 7) or the PNA-LNA (peptide nucleic acid–locked nucleic acid) polymerase chain reaction clamp (for exon 8) (12), we investigated the presence of the mutations in genomic DNA from 188 normal volunteers. The amplification signals were detected using Smart Cycler II (Cepheid, Sunnyvale, CA).

Microinjection into *Xenopus* oocytes

We subcloned cDNA of the wild-type *SLC34A2* and its mutants seen in the patients into pcDNA3.1, and capped RNA was transcribed *in vitro* from the T7 promoter. Integrity of RNA was confirmed by gel electrophoresis. Expression of the proteins on the surface of *Xenopus* oocytes and functional study were performed as described (13). In short, after being microinjected with 46 nl of water containing 46 ng of RNA, oocytes were then incubated in modified Barth's solution at 18°C for 3 d. In the phosphate transport assay, oocytes, seven for each injection group, were washed in Na^+-free ND-100 solution containing 0.5 mM KH_2PO_4 (25 mCi/ml ^{32}P-orthophosphoric acid) for 60 min. After washing three times with cold Na^+-free ND-100 solution (100 mM NaCl, 2 mM KCl, 1.8 mM $CaCl_2$, 1 mM $MgCl_2$, 5 mM *N*-2-hydroxyethylpiperazine-*N*′-ethane sulfonic acid [HEPES]), oocytes were lysed in 0.2 ml of 10% sodium dodecyl sulfate and the radioactivity was counted. In the electrophysiologic recording, whole-cell currents were measured using a conventional, 2-microelectrode-voltage clamp method with a holding potential of −50 mV. Under a continuous recording of current, oocytes were serially superfused with ND-100 solution (pH 6.6), ND-100 solution containing 1 mM NaH_2PO_4 (pH 6.6), and then ND-100 solution (pH 6.6).

In Situ Hybridization and Immunohistochemistry

Paraffin-embedded normal human lung tissue was serially thin sectioned, and we investigated the expression of *SLC34A2* RNA and surfactant protein A (SP-A). A part of the open reading frame of *SLC34A2* cDNA was amplified using primers tagged with the T7 promoter sequence. Fluorescent-labeled RNA probes were made using an RNA labeling kit (Hoffmann-La Roche, Basel, Switzerland). *In situ* hybridization was performed and the signal was detected by GenPoint fluorescein kit (Dako Cytomation, Glostrup, Denmark). SP-A protein was detected using a mouse anti-human SP-A monoclonal antibody (Dako Cytomation), together with a horseradish-labeled goat anti-mouse IgG antibody (Santa Cruz Biotechnology, Santa Cruz, CA) and 3,3′-diaminobenzidine chromogen.

RESULTS

We identified 6 cases of PAM from the case reports in Japan. Three patients were alive. Three had died; however, their paraffin-embedded tissues were available (Table 1 and Figure E1 of the online supplement). We were able to obtain samples from six of these patients (three still alive and three dead). Of the three live patients, two (patients 1 and 2) were children of parents who were first cousins. The other (patient 3) was from a family in which three patients were clustered and thus inbreeding was strongly suspected, considering that the inbreeding rate has been historically high in Japan (14). These three patients were unrelated and from different parts of Japan. To identify the gene responsible for PAM (the PAM gene) from a small number of samples, genomic DNA isolated from the peripheral blood of three live patients was investigated using the GeneChip mapping set (Affymetrix), which has the ability to analyze 100,000 SNPs at one time. The results were analyzed according to the homozygosity mapping strategy (6), which anticipates the candidate gene will be located in the homozygosity segment in which both copies of homologous chromosomes are derived from a single ancestral chromosome. To apply the strategy to genomewide SNP genotyping data, we took the following approach. We considered that the homozygosity segment could be detected as a stretch of homozygous SNPs (SHS) in which every SNP type is homozygous. We also considered that if the significance of SHS is appropriately defined, the homozygosity segment will be clearly delineated, and this should allow us to narrow the candidate region for the PAM gene geometrically by serially obtaining intersections of SHS for each patient. We defined significant SHS as a run of homozygous SNPs where the product of the frequencies of homozygosity reported in the Asian population for the individual SNPs is less than 1 in 100,000 (*see* the online supplement). Significant SHS of patients 1 through 3 are shown in Figures 2B–2D. A mathematical calculation revealed that the probability that the PAM gene is contained in significant SHS is 0.999 for the child of the first-cousin marriage and 0.94 even for the child

TABLE 1. PATIENTS' CHARACTERISTICS

	Sex	Alive/Dead Status	Inbreeding	PAM in Other Family Members	Sample Used	Other Information
Patient 1	F	Alive	Yes	Yes	Peripheral blood	Older sister of patient 4
Patient 2	M	Alive	Yes	Yes	Peripheral blood	
Patient 3	F	Alive	Uncertain	Yes	Peripheral blood	
Patient 4	F	Dead	Yes	Yes	Paraffin-embeded tissue	Younger sister of patient 1
Patient 5	F	Dead	NA	NA	Paraffin-embeded tissue	
Patient 6	F	Dead	NA	Yes	Paraffin-embeded tissue	

Except for patients 1 and 4, all patients were from different families and unrelated. NA = information not available.

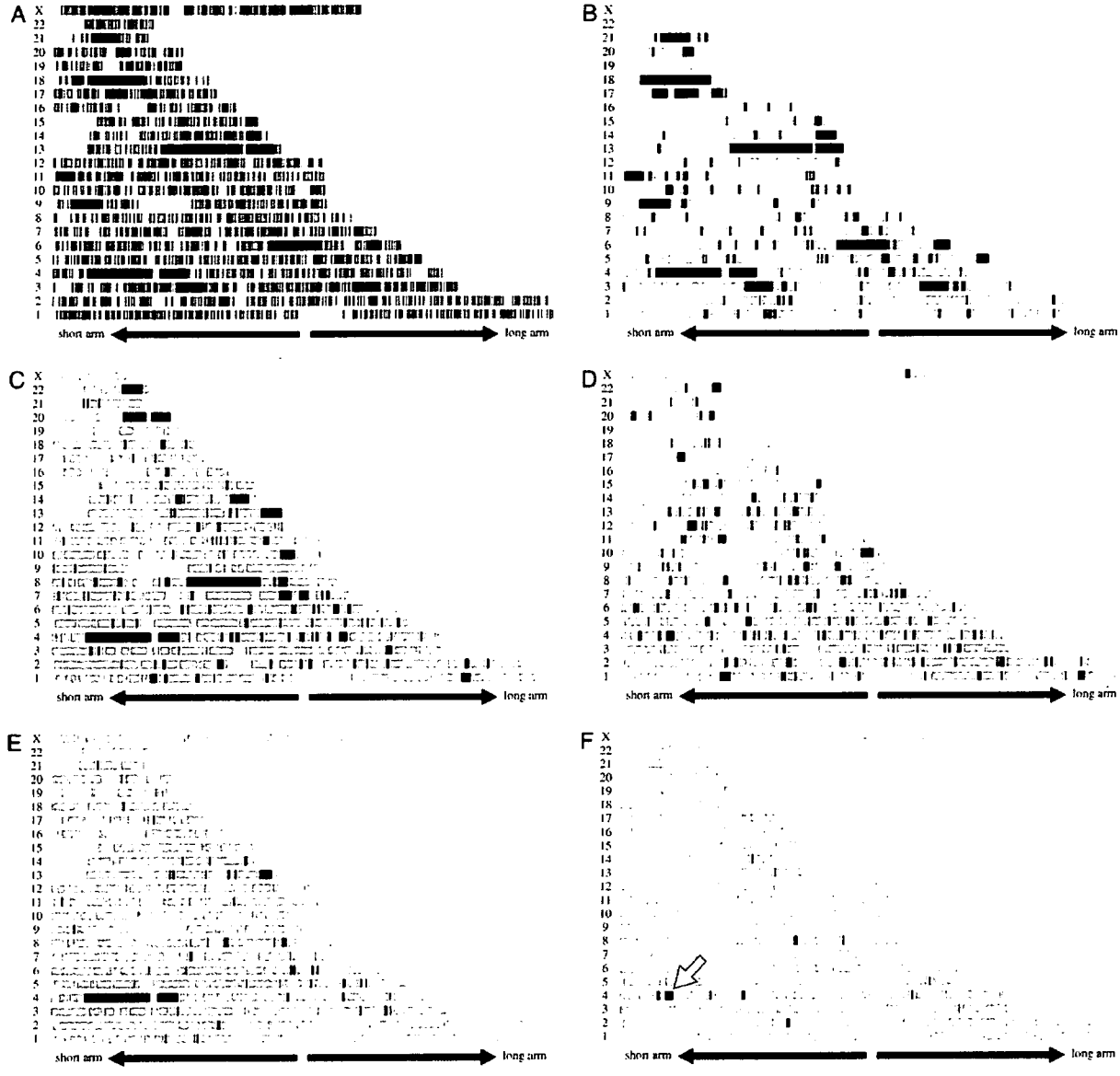

Figure 2. Narrowing the candidate chromosomal regions for the PAM gene using significant stretches of homozygous SNPs (SHS). (*A*) Result of SNP typing for patient 1. Each *vertical bar* indicates an SNP aligned according to its location on the chromosome. A homozygous SNP is shown in *black* and a heterozygous SNP is in *light gray*. *Gray arrows* under each panel indicate the direction of the short and the long arms of the chromosomes. (*B*) Significant SHS (shown in *black*) for patient 1 who is a child of a first-cousin marriage. (*C*) Significant SHS for patient 2. (*D*) Significant SHS for patient 3. (*E*) The overlap of significant SHS for patients 1 and 2. Data from only two patients considerably narrowed the candidate regions. (*F*) The overlap of significant SHS for patients 1, 2, and 3. An *arrow* indicates the significant SHS located on chromosome 4 that contained the PAM gene (*SLC34A2*).

of the 20th-cousin marriage (*see* Table E1). Consequently, the overlaps of significant SHS for patients 1 and 2 (Figure 2E) have a probability of 0.998 (= 0.999^2) of containing the PAM gene. We assumed the presence of the inbreeding in patient 3, and further narrowed the region, giving candidate regions with a total length of 12.4 Mb (*see* Table E2). The region contained 50 genes, of which 31 genes had known or suspected functions. *SLC34A2* (Unigene Hs. 479372: solute carrier family 34 [sodium phosphate], member 2) (15, 16), a transporter of sodium phosphate, was the only gene that was directly related to calcium or phosphate metabolism. We thus investigated the individual exons of *SLC34A2* and found that five of five patients had homozygous mutations, whereas 10 normal volunteers did not, indicating that a mutation in *SLC34A2* is significantly associated with PAM ($p < 2.5 \times 10^{-4}$ by the Fisher's exact test). To determine the frequency of the mutant genes in the Japanese population, we screened the genomic DNA from 188 volunteers (i.e., 376 control chromosomes) for the two mutations found, and all samples were negative. This indicates that the frequency of a chromosome with a mutant gene in the general population is less than 0.008 (a 95% confidence interval). In patients 3 and 5, an aberrant sequence replaced a part of exon 7 (Figure 3A), causing a frameshift that produces a truncated protein. In patients 1, 2, 4, and 6, a G nucleotide in the donor site of the splicing signal of exon 8 is

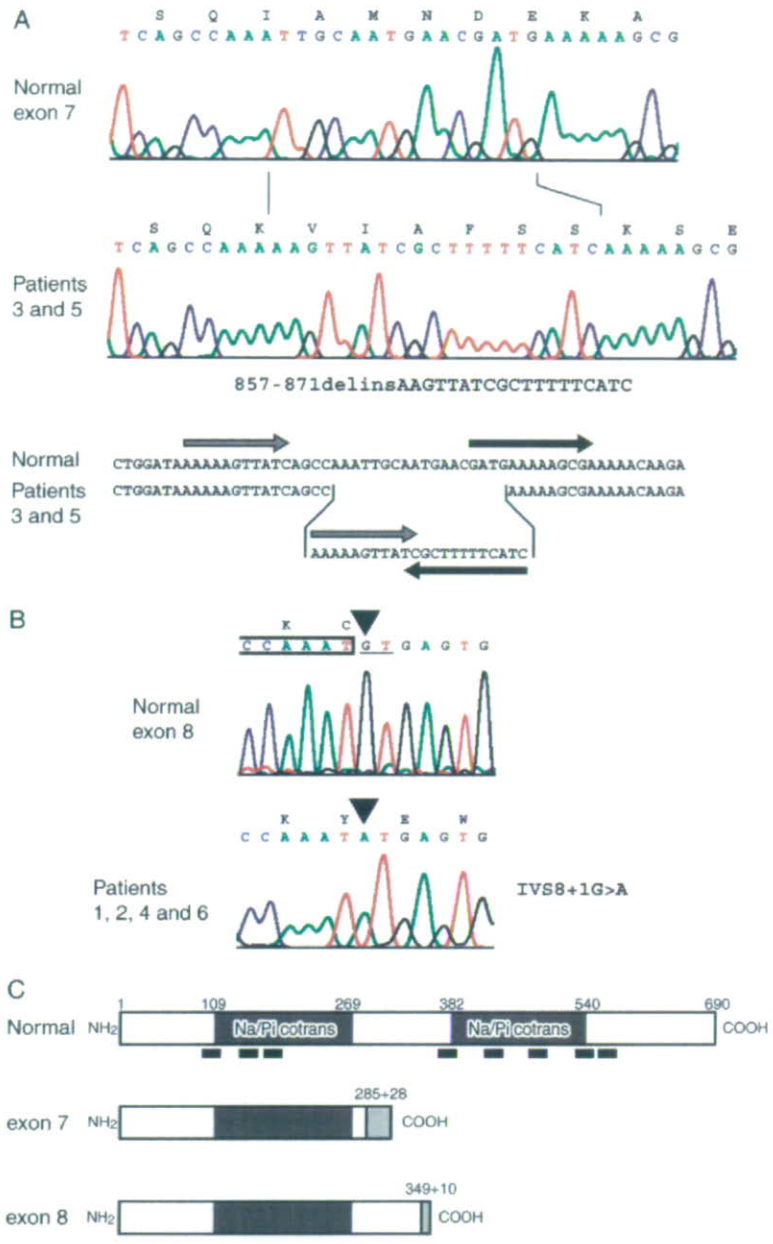

Figure 3. *SLC34A2* mutations in patients. (*A*) A deletion-insertion mutation in patients 3 and 5. Small duplications in the nucleotide sequence in the same (*gray arrows*) and in the opposite (*black arrows*) directions suggest a complicated mutation event. (*B*) Mutation observed in patients 1, 2, 4, and 6. The 3′ end of the exon 8 sequence is enclosed with a translated amino acid sequence shown *above*. A conserved splicing donor sequence (GT) is *underlined*. *Solid, inverted triangles* indicate the point of mutation resulting in a G to A transition. The nucleotide change abrogates normal splicing and the translation continues into intron 8 to add 10 aberrant amino acids before being terminated by an occasional stop codon. (*C*) Mutant proteins predicted from the mutant sequences. Structures of normal protein and protein produced by the mutation in exon 7 and in exon 8 are depicted. Na/Pi cotrans = a sodium phosphate cotransporter motif (pfam 02,690). *Black boxes* under normal protein are predicted transmembrane domains. Numbers shown on mutant proteins are (numbers of *SLC34A2*-derived amino acids in the mutant protein) plus (numbers of aberrant amino acids added by a frameshift resulting from a mutation). Sequences that exist only in the mutant proteins are indicated by *light-gray boxes*.

replaced with an A (Figure 3B), which causes splicing failure, leading to a premature termination of the protein. The truncated proteins are about half the size of the full-length protein (Figure 3C). Patients 1 and 2 shared a conserved haplotype in a 1.1-Mb–long region, whereas patients 3 and 5 shared a 150-kb–long region (Figure 4). This suggests that each mutation is derived from a single founder.

Because *SLC34A2* is a membrane protein with eight predicted transmembrane domains, proteins lacking five of these domains are likely to lose the normal function. To confirm this, we cloned the wild-type and the mutant *SLC34A2* cDNA individually into the pcDNA3.1 vector (Invitrogen, Carlsbad, CA). Capped RNA was transcribed *in vitro* from the T7 promoter and microinjected into the oocytes of *Xenopus laevis*. The wild-type *SLC34A2* transported phosphate in the presence of sodium, whereas the mutants did not (Figure 5A). *SLC34A2* cotransports sodium and phosphate into the cells (15) with a stoichiometry of $3Na^+$:$1HPO_4^{2-}$, and thus produces inward current. The wild-type *SLC34A2* elicited inward current with the addition of NaH_2PO_4, whereas mutants did not (Figure 5B). The proteins with the mutations seen in the patients abolished the normal transporter function.

DISCUSSION

SLC34A2 is expressed mainly in lung and mammary gland and to a lesser extent in intestine, kidney, and prostate (15). *SLC34A2* is the only phosphate transporter that is highly expressed in the lung (15), where the expression is observed specifically in type II alveolar cells (Figure 6) (17). By immunohistochemistry, *SLC34A2* protein was observed in the apical pole of the cells (18). The type II cells produce pulmonary surfactant, of which phospholipids are essential constituents. Outdated surfactant is taken up by type II cells for recycling and degradation and by

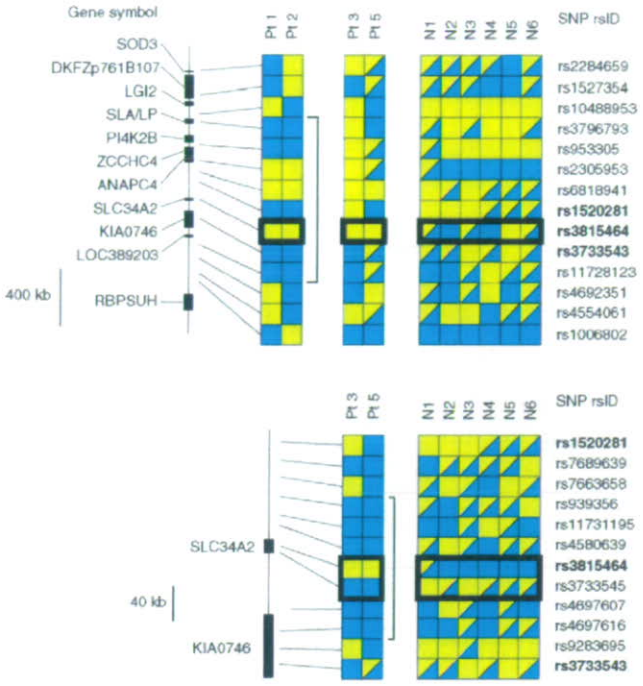

Figure 4. Haplotype analysis of the patients. Coarse scale (*upper panel*) and fine scale (*lower panel*) analyses are shown. We individually amplified each SNP site and genotyped by sequencing. Samples of patients 4 and 6 were excluded from the analysis: patient 4 is the younger sister of patient 1 and the same haplotype was expected. DNA of sufficient quality was not obtained from the paraffin-embedded tissue of patient 6 for completion of all SNP analyses. Regions conserved for patients 1 and 2 or for patients 3 and 5 are indicated by *brackets*. All SNPs have a minor allele frequency of more than 0.2. *Blue* and *yellow squares* show common alleles and rare alleles, respectively. Heterozygous sites are indicated by both colors. SNP sites included in the *SLC34A2* gene are *boxed*. SNP rsIDs used in both coarse and fine analyses are in *bold letters*. N = normal control; Pt = patient. The headings Gene symbol and SNP rsID indicate, respectively, the official symbol and an SNP ID used in the Genbank database (www.ncbi.nlm.nih.gov).

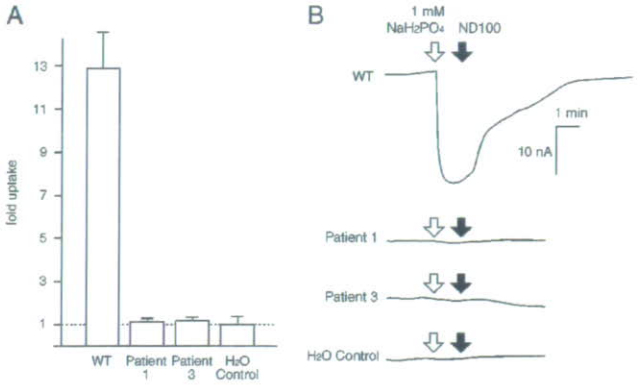

Figure 5. Functional analysis of *SLC34A2* mutants. (*A*) Phosphate transport assay. *Xenopus* oocytes microinjected with transcribed *in vitro* wild-type RNA, mutant RNA, or water were assayed for phosphate uptake. (*B*) Electrophysiologic measurement. Microinjected oocytes superfused in ND-100 solution (pH 6.6; 100 mM NaCl, 2 mM KCl, 1.8 mM $CaCl_2$, 1 mM $MgCl_2$, 5 mM *N*-2-hydroxyethylpiperazine-*N'*-ethane sulfonic acid [HEPES]) were exposed to ND-100 solution containing 1 mM NaH_2PO_4 (pH 6.6) (*open arrows*) and then washed with ND-100 solution (pH 6.6) (*solid arrows*). Patient 1, Patient 3 = mutants observed in patients 1 and 3; WT = wild type.

alveolar macrophages for degradation (19). Degraded phospholipids release phosphate that should be cleared from the alveolar space. Dysfunction of *SLC34A2* may reduce the clearance of phosphate and may lead to the formation of microliths. In many cases of PAM, the lung is the only organ affected (1–3). Other organs may have phosphate transporters with redundant functions.

We have demonstrated that (*1*) homozygous inactivating mutations in *SLC34A2* are present in patients with PAM, (*2*) *SLC34A2* is highly expressed in alveolar type II cells, and (*3*) loss of the normal function of *SLC34A2* can explain the pathophysiology of PAM. On the basis of this evidence, we conclude that *SLC34A2* is the PAM gene.

Recently, Corut and colleagues (20) reported that *SLC34A2* is mutated in Turkish patients with PAM. The result is consistent with ours and confirms that *SLC34A2* is the causative gene for PAM.

No effective treatment for PAM currently exists, with the exception of lung transplantation. Disodium etidronate inhibits microcrystal growth of hydroxyapatite and thus inhibits ectopic calcification. This drug has been used to treat PAM, with little or no benefit (21–23). Our results suggest that remedies that

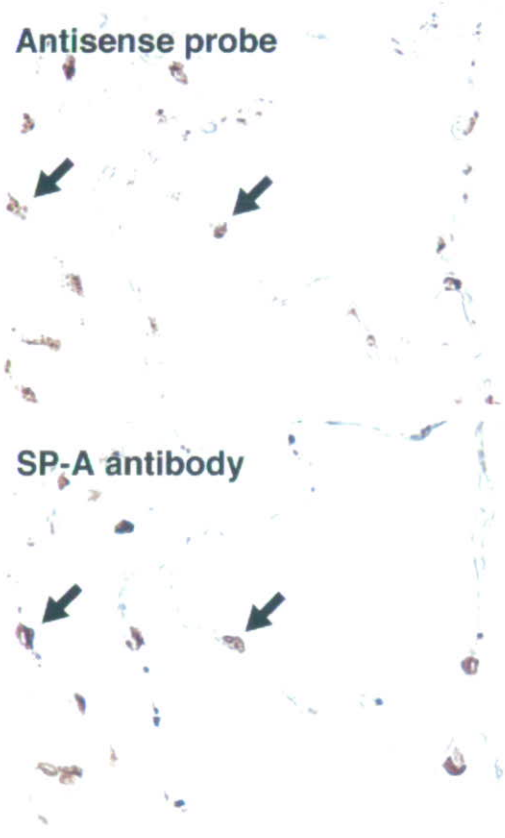

Figure 6. In situ hybridization. Cells expressing *SLC34A2* were investigated using serial sections of normal lung tissue. *Antisense probe*: *in situ* hybridization using *SLC34A2* antisense probe. *SP-A antibody*: immunohistochemical detection of SP-A (a marker of type II alveolar cells). *Arrows* indicate cells detected by both methods.

target phosphate metabolism rather than calcium metabolism may be beneficial for the treatment of PAM.

Conflict of Interest Statement: None of the authors has a financial relationship with a commercial entity that has an interest in the subject of this manuscript.

Acknowledgment: The authors thank Dr. Roger Reddel, Children's Medical Research Institute, Sydney, Australia, for his helpful collaboration. They thank Dr. Yasushi Okazaki for detailed scientific discussion.

References

1. Sosman MC, Dodd GD, Jones DW. The familial occurrence of pulmonary alveolar microlithiasis. *AJR Am J Roentgenol* 1957;77:947–1012.
2. Ucan ES, Keyf AI, Aydilek R, Yalcin Z, Sebit S, Kudu M, Ok U. Pulmonary alveolar microlithiasis: review of Turkish reports. *Thorax* 1993;48:171–173.
3. Mariotta S, Ricci A, Papale M, De Clementi F, Sposato B, Guidi L, Mannino F. Pulmonary alveolar microlithiasis: report on 576 cases published in the literature. *Sarcoidosis Vasc Diffuse Lung Dis* 2004; 21:173–181.
4. Puhr L. Mikrolithiasis alveolaris pulmonum. *Virchows Arch Pathol Anat Physiol Klin Med* 1933;290:156–160.
5. Tachibana T, Hayashi S, Jokoh T, Ueda S, Takahashi H. Diagnosis and management of pulmonary alveolar microlithiasis. *Sarcoidosis Vasc Diffuse Lung Dis* 2001;18:58.
6. Lander ES, Botstein D. Homozygosity mapping: a way to map human recessive traits with the DNA of inbred children. *Science* 1987;236: 1567–1570.
7. Huqun, Izumi S, Uchiyama B, Tanaka S, Tazawa R, Ishida T, Nukiwa T, Yoshimura K, Kudo K, Tachibana T, *et al.* GeneChip analysis of genomic DNA from patients with pulmonary alveolar microlithiasis [abstract]. *Respirology* 2004;9(Suppl):A155.
8. Huqun, Izumi S, Uchiyama B, Tanaka S, Ishida T, Tazawa R, Kanazawa M, Yoshimura K, Nukiwa T, Tachibana T, *et al.* Identification of the candidate region for the responsible gene of the pulmonary alveolar microlithiasis using a genome-wide SNP analysis [abstract]. *J Jpn Respir Soc* 2005;43(Suppl):174.
9. Huqun, Izumi S, Miyazawa H, Uchiyama B, Tanaka S, Ishida T, Nagai A, Tanaka T, Fukuyama S, Tazawa R, *et al.* Identification of a chromosome location linked to pulmonary alveolar microlithiasis (PAM) [abstract]. *Eur Respir J* 2005;26(Suppl 49):269s.
10. Hagiwara K, Huqun, Izumi S, Miyazawa H, Uchiyama B, Ishida T, Tanaka S, Tazawa R, Fukuyama S, Tanaka T, *et al.* The autozygous segments predicted by a genome-wide SNP typing revealed mutations in the type IIb sodium phosphate co-transporter (SLC34A2) causing pulmonary alveolar microlithiasis [abstract]. *Proc Am Thorac Soc* 2006;3:A102.
11. Huqun, Izumi S, Miyazawa H, Uchiyama B, Ishida T, Tanaka S, Tazawa R, Fukuyama S, Tanaka T, Nagai Y, *et al.* Identification of the responsible gene for the pulmonary alveolar microlithiasis using a genome-wide SNP analysis [abstract]. *J Jpn Respir Soc* 2006;44(Suppl):122.
12. Nagai Y, Miyazawa H, Huqun, Tanaka T, Udagawa K, Kato M, Fukuyama S, Yokote A, Kobayashi K, Kanazawa M, *et al.* Genetic heterogeneity of the epidermal growth factor receptor (EGFR) in non-small cell lung cancer cell lines revealed by a rapid and sensitive detection system, the PNA-LNA PCR clamp. *Cancer Res* 2005; 65:7276–82.
13. Lin C, Nagai M, Ishigaki D, Hayasaka K, Endoh M, Ishii K. Cross-talk between beta(1)-adrenoceptors and ET(A) receptors in modulation of the slow component of delayed rectifier K(+) currents. *Naunyn Schmiedebergs Arch Pharmacol* 2005;371:133–140.
14. Imaizumi Y. A recent survey of consanguineous marriages in Japan. *Clin Genet* 1986;30:230–233.
15. Feild JA, Zhang L, Brun KA, Brooks DP, Edwards RM. Cloning and functional characterization of a sodium-dependent prostate transporter expressed in human lung and small intestine. *Biochem Biophys Res Commun* 1999;258:578–582.
16. Xu H, Bai L, Collins JF, Ghishan FK. Molecular cloning, functional characterization, tissue distribution, and chromosomal localization of a human, small intestinal sodium-phosphate (Na+-Pi) transporter (SLC34A2). *Genomics* 1999;62:281–284.
17. Hashimoto M, Wang DY, Kamo T, Zhu Y, Tsujiuchi T, Konishi Y, Tanaka M, Sugimura H. Isolation and localization of type IIb Na/Pi cotransporter in the developing rat lung. *Am J Pathol* 2000;157:21–27.
18. Traebert M, Hattenhauer O, Murer H, Kaissling B, Biber J. Expression of type II Na-P(i) cotransporter in alveolar type II cells. *Am J Physiol* 1999;277:L868–L873.
19. Poelma DL, Ju MR, Bakker SC, Zimmermann LJ, Lachmann BF, van Iwaarden JF. A common pathway for the uptake of surfactant lipids by alveolar cells. *Am J Respir Cell Mol Biol* 2004;30:751–758.
20. Corut A, Senyigit A, Ugur S, Altin S, Ozcelik U, Calisir H, Yildirim Z, Gocmen A, Tolun A. Mutations in SLC34A2 cause pulmonary alveolar microlithiasis and are possibly associated with testicular microlithiasis. *Am J Hum Genet* 2006;79:650–656.
21. Göcmen A, Toppare MF, Kiper N, Buyukpamukcu N. Treatment of pulmonary alveolar microlithiasis with a diphosphonate–preliminary results of a case. *Respiration* 1992;59:250–252.
22. Jankovic S, Pavlov N, Ivkosic A, Erceg I, Glavina-Durdov M, Tocilj J, Dragisic-Ivulic S, Primorac D. Pulmonary alveolar microlithiasis in childhood: clinical and radiological follow-up. *Pediatr Pulmonol* 2002; 34:384–387.
23. Mariotta S, Guidi L, Mattia P, Torrelli L, Pallone G, Pedicelli G, Bisetti A. Pulmonary microlithiasis: report of two cases. *Respiration (Herrlisheim)* 1997;64:165–169.

Original Paper

International Archives of Allergy and Immunology

Int Arch Allergy Immunol 2007;143(suppl 1):44–49
DOI: 10.1159/000101404

Published online: May 31, 2007

Theophylline Attenuates the Neutrophil-Dependent Augmentation of Eosinophil Trans-Basement Membrane Migration

Izumi Kikuchi Shinya Kikuchi Takehito Kobayashi Yotaro Takaku
Koichi Hagiwara Minoru Kanazawa Makoto Nagata

Department of Respiratory Medicine, Saitama Medical University, Saitama, Japan

Key Words
Neutrophils · Eosinophils · Theophylline · Interleukin-8 · Cell migration

Abstract
Background: Recent evidence suggests that both neutrophilic and eosinophilic inflammation persist in the airways of patients with severe asthma. Neutrophils can secrete a variety of mediators which may augment the migration of eosinophils. We have reported that activated neutrophils augment the trans-basement membrane migration (TBM) of eosinophils in vitro. Theophylline has been shown to modulate some functions of both neutrophils and eosinophils. The objective of this study was to evaluate whether theophylline modulates the neutrophil-dependent augmentation of eosinophil TBM. ***Methods:*** Eosinophils and neutrophils were isolated from peripheral blood collected from healthy donors and were then preincubated with either 0.1 mM theophylline or the medium control. The TBM of eosinophils in response to IL-8 was evaluated in the presence or absence of neutrophils by using the chambers with a Matrigel®-coated Transwell® insert. The generation of O_2^- was evaluated by the cytochrome c reduction assay. ***Results:*** As previously reported, IL-8-stimulated neutrophils significantly augmented the TBM of eosinophils. Theophylline significantly attenuated the neutrophil-dependent augmentation of eosinophil TBM ($p < 0.001$) and did not directly modify the TBM of neutrophils in response to IL-8 or LTB4. Similarly, the LTB4-induced TBM of eosinophils was not modified by theophylline. Finally, theophylline attenuated the superoxide anion generation from IL-8-stimulated neutrophils on the Matrigel-coated plates. ***Conclusions:*** Our results show that theophylline can attenuate the neutrophil-dependent augmentation of eosinophil TBM. This effect is possibly attributable to the suppression of neutrophil activation provoked by the combination of basement membrane and IL-8.

Introduction

Traditionally, theophylline has been used as a bronchodilator in the treatment of asthma. However, this drug appears to reduce the tissue infiltration of eosinophils, predominant inflammatory cells in the airways of asthmatic patients [1–3]. For example, Sullivan et al. [1] reported that theophylline attenuates the airway accumulation of eosinophils in response to allergen inhalation in atopic asthma. More recently, Aizawa et al. [2] showed that theophylline eventually reduced the percentage of eosinophils in induced sputum from patients with

KARGER
Fax +41 61 306 12 34
E-Mail karger@karger.ch
www.karger.com

1018–2438/07/1435–0044$23.50/0

Accessible online at:
www.karger.com/iaa

Correspondence to: Dr. Makoto Nagata
Department of Respiratory Medicine, Saitama Medical University
38 Morohongou, Moroyama-cho, Iruma-gun
Saitama 350-0495 (Japan)
Tel. +81 492 76 1319, Fax +81 492 95 8399, E-Mail favre4mn@saitama-med.ac.jp

mild-to-moderate asthma. Finally, Lim et al. [3] reported that theophylline reduced the number of eosinophils in sputa, biopsied specimens, and bronchoalveolar lavage fluids in mild asthmatic patients. Theophylline actually possesses a variety of in vitro effects on human eosinophils: induction of apoptosis [4, 5], inhibition of degranulation [5–7] and cell migration [8], and reduction of the surface expression of CD11b [6, 7, 9] or CD4 [8]. In this context, we have reported that theophylline attenuates eosinophil adhesion to endothelial cells in vitro at a clinically therapeutic concentration [9]. Furthermore, theophylline inhibits the expression of ICAM-1 and VCAM-1 on endothelial cells which had been stimulated with interleukin-4 (IL-4) plus tumor necrosis factor-α (TNF-α) [9, 10]. Thus, theophylline possibly exerts an inhibitory effect on both the adhesive property of eosinophils and the expression of adhesion molecules on endothelial cells [9, 10].

In a subgroup of patients with asthma, the accumulation of neutrophils is found in their airways even in the absence of infection. Asthma in such patients is often severe and chronic and is refractory to corticosteroid therapy [11–14]. Based upon a report from the European Network Study for Understanding Mechanisms of Severe Asthma (ENFUMOSA), patients with severe asthma have a higher percentage of neutrophils in sputum and present evidence of the continuing release of eosinophil-derived mediators in comparison to patients with mild-to-moderate asthma, suggesting that both neutrophilic and eosinophilic inflammation persist in the airways of patients with severe asthma [14]. In this context, we have reported a positive correlation between the concentrations of neutrophils and eosinophils in induced sputum from patients with severe persistent asthma who were treated with medicines including systemic corticosteroids [15]. Concentrations of IL-8 which acts as a chemoattractant for neutrophils have been shown to be correlated with the accumulation of neutrophils in the airways of patients with asthma [16], and this chemokine may therefore be an essential molecule responsible for the development of neutrophilic inflammation in asthma. We recently published that, when eosinophils were coincubated with neutrophils and stimulated with IL-8 in vitro, the trans-basement membrane migration (TBM) of eosinophils was significantly induced [17]. This augmented TBM of eosinophils by neutrophils was inhibited by a matrix metalloproteinase-9 inhibitor, a leukotriene B4 receptor antagonist, or platelet activating factor antagonists [17]. This provides a mechanism for the relationship between neutrophils and eosinophils in severe asthma and raises a possibility that therapies which suppress the interaction between neutrophils and eosinophils may be effective for severe asthma.

The objective of this study was to evaluate whether theophylline modulates the neutrophil-dependent augmentation of the eosinophil TBM.

Materials and Methods

Reagents

Percoll® was obtained from Pharmacia (Uppsala, Sweden). Anti-CD16 antibody-coated magnetic beads were purchased from Miltenyl Biotec (Auburn, Calif., USA). RPMI 1640 medium, PBS, newborn calf serum (NCS) and fetal calf serum (FCS) were obtained from Life Technologies (Grand Island, N.Y., USA). Recombinant human (rh-) IL-8 was purchased from R&D Systems (Minneapolis, Minn., USA). Leukotriene B4 (LTB4) was purchased from Cayman Chemical (Ann Arbor, Mich., USA). O-Phenylenediamine (OPD) and BSA were obtained from Sigma (St. Louis, Mo., USA). The acetoxy methyl ester of 2′-7′-bis (2-carboxy-ethyl)-5(6)-carboxyfluorescein (BCECF-AM) was purchased from Dojin Laboratory (Kumamoto, Japan). Other reagents were purchased from Sigma (St. Louis, Mo., USA) unless otherwise specified.

Preparation of Neutrophils and Eosinophils

Neutrophils and eosinophils were isolated from peripheral blood collected from nonatopic healthy donors whose eosinophil content was less than 5% of their peripheral leukocytes [17]. Informed consent was obtained prior to the collection of each blood sample. Neutrophils and eosinophils were separated by the combination of Percoll density-gradient centrifugation and negative immunomagnetic bead selection as previously described [17]. Briefly, 40 ml of dextran were added to 160 ml of heparinized blood, and erythrocytes were removed as sediments. The remaining suspension of leukocytes was layered onto Percoll gradients of 1.080, 1.085, and 1.090 g/ml in density. After centrifugation at 700 *g* for 20 min, neutrophils (purity exceeded 95%) were collected from 1.085/1.090 g/ml interface and were then suspended in HBSS containing 0.2% BSA (HBSS/BSA buffer). Following the removal of Percoll, the red blood cells in the pellet were lysed by hypotonic shock and were then removed by washing with cold PBS. The remaining cells were washed with 4°C HBSS supplemented with 2% NCS (HBSS/NCS), incubated with anti-CD16 antibody-coated magnetic beads for 30 min at 4°C and were then filtered with a column containing steel wool placed in a magnetic field (Miltenyl Biotec). Eosinophils (> 98% purity and > 99% viability), which passed through the column, were collected and washed, and the number of cells was adjusted to 2.5×10^5 cells/ml by using the HBSS/BSA buffer.

Trans-Basement Membrane Migration

The TBM of neutrophils and eosinophils was examined using a modified Boyden's chamber method [17]. The study was conducted in duplicate. Briefly, neutrophils or eosinophils were precultured in the presence or absence of a clinically relevant concentration of 0.1 mM theophylline at 37°C for 20 min before the each study. Neutrophils were fluorescent-labeled with BCECF-AM. La-

beled neutrophils (0.5×10^5 cells), eosinophils (0.5×10^5 cells), or a combination thereof (0.5×10^5 cells plus 0.5×10^5 cells) in a 200-μl medium, was added to the upper compartment of a chamber with a Matrigel®-coated Transwell® insert (pore size 3 μm, Becton Dickinson Labware, N.Y., USA). Either the control medium (500 μl) or a medium which contained one of activators (IL-8 and LTB4) was added to the lower compartment of the chamber. After a 2-hour incubation in 5% CO_2 at 37°C, the medium in the upper compartment of the chamber and the inserts between the chambers were gently removed. The peroxidase activity of eosinophils in the medium in the lower compartment of the chamber was determined, and the number of migrated eosinophils was calculated from the activity of the standard media which contained known numbers (5×10^3, 1.5×10^4, 5×10^4, 1.5×10^5 and 5×10^5 cells) of eosinophils. To determine the peroxidase activity of eosinophils, the medium was incubated with a substrate (1 mM OPD, 1 mM H_2O_2, and 0.1 % Triton X-100 in Tris-HCl, pH 8.0) for 30 min at room temperature [17]. The reaction was stopped by adding 100 μl of 4 N H_2SO_4, and absorbance at 490 nm was determined. The numbers of migrated neutrophils were determined by the measurement of fluorescence in the medium using the Fluoromark® (Bio-Rad Laboratories, Calif., USA) microplate fluorometer [17]. The viability of both eosinophils and neutrophils after migration exceeded 98% by trypan blue exclusion.

Superoxide Anion (O_2^-) Generation

The neutrophil O_2^- generation was measured as the SOD-inhibitable reduction of ferricytochrome c, as described previously [18], in 96-well culture plates (Corning Inc., Corning, New York, N.Y., USA) coated with Matrigel. We initially added SOD (0.2 mg/ml in HBSS/gel; 20 μl) to SOD control wells and then HBSS/gel to all wells to obtain the final volume to 100 μl. Neutrophil density was adjusted to 1.25×10^6 cells/ml of HBSS/gel, and this suspension was mixed with cytochrome c at 4:1 (12 mg/ml of HBSS/gel). Neutrophils, which were preincubated with either 0.1 mM theophylline or the buffer alone (control) at 37°C for 20 min, were then added to all wells at a volume of 100 μl. To initiate the reaction, the cells were incubated with IL-8 (10 nM). Immediately after adding the activator, absorbance of the cell suspensions in the wells was measured at 550 nm in an IMMUNO-MINI (NJ-2300; Japan Intermed Co., Tokyo, Japan), followed by repeated readings over the next 240 min. Between readings, the plates were placed in a 5% CO_2 incubator at 37°C. Each reaction was performed in duplicate against an identical control reaction containing 20 μg/ml SOD. The results were adjusted to represent a 1-ml reaction volume, and the O_2^- generation was calculated at an extinction coefficient of 21.1×10^3 M/l^{-1} cm^{-1} as nanomoles of cytochrome c reduced per 1.0×10^6 cells per minute minus the SOD control. The maximum value during the incubation time was examined for the effects of drugs on eosinophil O_2^- generation. Cell viability as determined by trypan blue exclusion at the completion of each experiment remained at 95% after 240 min of incubation.

Statistical Analysis

Values are expressed as mean ± SEM. Repeated-measures ANOVA was conducted to compare variables. When the initial p value was below 0.05, Scheffé's posthoc test was conducted to determine the significant difference between groups. Student's t test was conducted to make paired comparisons. $p < 0.05$ was considered statistically significant.

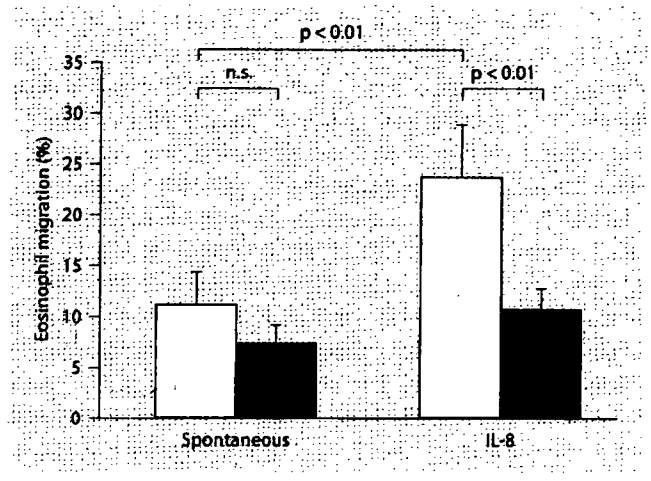

Fig. 1. Effects of 0.1 mM theophylline on the spontaneous (left panel) or 10 nM IL-8 (right panel)-induced trans-basement migration of eosinophils in the presence of neutrophils. Open bars represent the control (no drug), and closed bars represent cells incubated with theophylline. Values are expressed as mean ± SEM of 10 experiments.

Results

Effects of Theophylline on the TBM of Eosinophils Induced by a Combination of IL-8 and Neutrophils

As previously reported [17], IL-8 (10 nM) alone or the presence of neutrophils alone does not induce the TBM of eosinophils. However, a combination of IL-8 and neutrophils significantly induces the TBM of eosinophils (data not shown).

To evaluate whether theophylline modulates the neutrophil-dependent augmentation of the eosinophil TBM, neutrophils and eosinophils were precultured in the presence or absence of a clinically relevant concentration of 0.1 mM theophylline at 37°C for 20 min; the TBM assay was then performed. Consequently, the spontaneous TBM of eosinophils in the presence of neutrophils was not modified by 0.1 mM theophylline (fig. 1). However, the enhanced TBM of eosinophils induced by a combination of IL-8 and neutrophils was significantly reduced by 0.1 mM theophylline (fig. 1).

Theophylline Does Not Directly Modulate the TBM of Neutrophils or Eosinophils

To examine whether the inhibitory effect of theophylline on the neutrophil-dependent augmentation of the eosinophil TBM occurs through the attenuation of the TBM of either neutrophils or eosinophils, the effects of

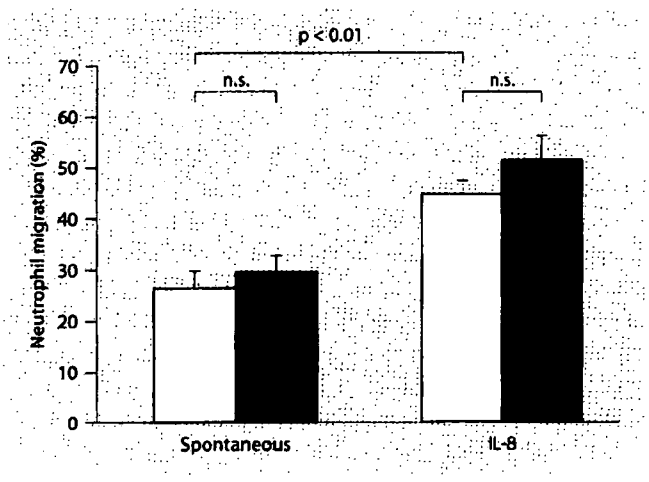

Fig. 2. Effects of 0.1 mM theophylline on the spontaneous (left panel) or 10 nM IL-8 (right panel)-induced trans-basement migration of neutrophils. Open bars represent the control, and closed bars represent cells incubated with 0.1 mM theophylline. Values are expressed as mean ± SEM of 6 experiments.

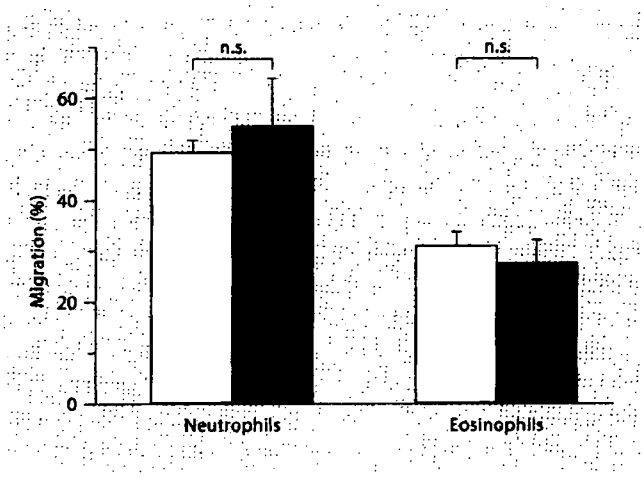

Fig. 3. Effects of 0.1 mM theophylline on the 30 nM LTB4-induced trans-basement migration of neutrophils (left panel) or eosinophils (right panel). Open bars represent the control, and closed bars represent cells incubated with 0.1 mM theophylline. Values are expressed as mean ± SEM of 6 experiments.

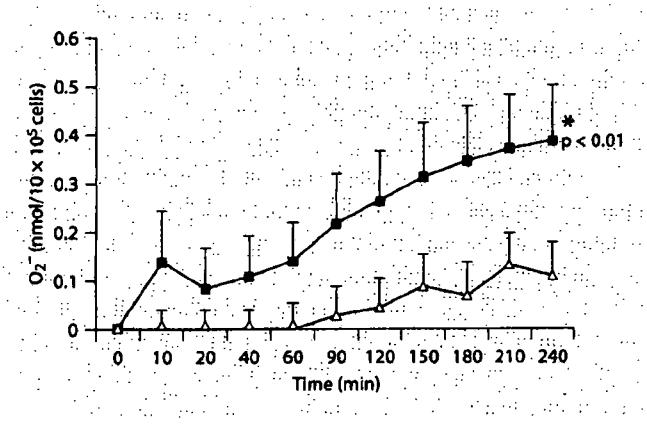

Fig. 4. Effects of theophylline on the superoxide anion generation from neutrophils incubated in 96-well culture plates coated with Matrigel and activated with 10 nM IL-8. Closed squares represent the control, and open triangles represent cells incubated with 0.1 mM theophylline. Values are expressed as mean ± SEM of 6 experiments.

theophylline on the TBM of each cell type were evaluated. Theophylline, at a concentration where it can attenuate the neutrophil-induced TBM of eosinophils, does not modify the spontaneous or IL-8-induced TBM of neutrophils (fig. 2). Similarly, theophylline does not modify the LTB4-induced TBM of neutrophils or eosinophils (fig. 3). Therefore, the inhibitory effect of theophylline on the TBM of eosinophils (fig. 1) is unlikely due to the direct effect on the migrative response of neutrophils or eosinophils.

Theophylline Inhibits the O_2^- Generation from Activated Neutrophils

Theophyline may reduce the TBM of eosinophils through the inhibition of activation and release of mediators from neutrophils. To test this hypothesis, neutrophils were preincubated in the presence or absence of 0.1 mM theophylline at 37°C for 20 min; subsequently, the O_2^- generation was evaluated in 96-well culture plates coated with Matrigel. In these experimental settings, neutrophils did not spontaneously generate O_2^-. However, neutrophils generated O_2^- in the presence of 10 nM IL-8, and the generation was significantly attenuated by theophylline (fig. 4).

Discussion

We found that a therapeutically relevant concentration of theophylline attenuated the TBM of eosinophils which is enhanced by neutrophils. The inhibitory effect of theophylline was not attributable to the direct effect on

the migratory response of neutrophils or eosinophils, since the drug modified the TBM of neither neutrophils induced by IL-8 or LTB4, nor eosinophils induced by LTB4. On the other hand, theophylline attenuated the IL-8-induced generation of O_2^- in the presence of a basement membrane component. Collectively, these results suggest that theophylline attenuates the neutrophil-dependent mechanism in the augmentation of the eosinophil TBM which may be important in the airways of patients with severe asthma [13–15].

Activated neutrophils can secrete a variety of mediators, e.g. matrix metalloproteinases, LTB4, platelet-activating factor, and TNF-α, which can induce the digestion of basement membrane or the migration or activation of eosinophils [19, 20], thus possibly attributing to the pathophysiology of asthma. Our observations indicated that a combination of IL-8 and a basement membrane component induced neutrophil respiratory burst which is inhibited by theophylline. The biological consequences of oxygen species released from inflammatory cells would modify either the morphological or functional status of the endothelium such as permeability, adhesion molecule expression, and adhesiveness to leukocytes [21–23]. More importantly, oxygen species alter the functional status of leukocytes. For example, we and others have reported that hydrogen peroxide promotes eosinophil and neutrophil adhesion via β_2 integrins [24, 25]. Therefore, the inhibitory effect of theophylline on the enhanced TBM of eosinophils seems, at least in part, attributable to the suppression of neutrophil activation and mediator release provoked by a combination of basement membrane and chemoattractants such as IL-8. Functions of neutrophils are not effectively suppressed by corticosteroids [26, 27], suggesting that neutrophils may play a role in the pathophysiology of asthma even under corticosteroid treatment. Classically, theophylline has been used as a bronchodilator to control the smooth muscle tone of the airways of asthmatics. More recently, however, theophylline has been shown to have a variety of inhibitory effects on inflammatory cells involved in asthmatic inflammation. In clinical settings, there is increasing evidence that the use of theophylline attenuates the eosinophil accumulation in the airways of asthmatic patients [1–3]. Our observations provide evidence of the novel modulatory effects of theophylline on the interactions between neutrophils and eosinophils as a mechanism for the attenuation of eosinophil accumulation in the airways of asthmatics, especially in patients with severe disease. Although the exact impact of this anti-inflammatory property of theophylline on its clinical effects remains to be elucidated, it is plausible that theophylline exerts inhibitory effects on both eosinophils directly and inflammatory networks such as the interaction between neutrophils and eosinophils. The combination of inhaled or oral corticosteroids and theophylline has been shown to provide additive clinical and physiological effects in moderate to severe asthma [28, 29], suggesting that these two classes of drugs act via differential mechanisms to modulate airway changes in asthma. Theophylline would alter both bronchial smooth muscle tone and the accumulation and/or functional state of eosinophils via a complex of mechanisms including intervention on the interaction between neutrophils and eosinophils, and may therefore provide clinical benefits additionally to corticosteroids in the treatment of asthma.

In conclusion, we found here that theophylline attenuates the neutrophil-dependent augmentation of the eosinophil TBM mainly via the suppression of neutrophil activation provoked by a combination of basement membrane and IL-8. This provides a novel mechanism of theophylline effects and raises a possibility that theophylline suppresses the interaction between neutrophils and eosinophils which may be important in the pathophysiology of severe asthma.

References

1 Sullivan P, Bekir S, Jaffar Z, Page C, Jeffery P, Costello J: Anti-inflammatory effects of low-dose oral theophylline in atopic asthma. Lancet 1994;343:1006–1008.

2 Aizawa H, Iwanaga T, Inoue H, Takata S, Matsumoto K, Takahashi N, Yoshida M, Hara N: Once-daily theophylline reduces serum eosinophil cationic protein and eosinophil levels in induced sputum of asthmatics. Int Arch Allergy Immunol 2000;121:123–128.

3 Lim S, Tomita K, Carramori G, Jatakanon A, Oliver B, Keller A, Adcock I, Chung KF, Barnes PJ: Low-dose theophylline reduces eosinophilic inflammation but not exhaled nitric oxide in mild asthma. Am J Respir Crit Care Med 2001;164:273–276.

4 Ohta K, Sawamoto S, Nakajima M, Kubota S, Tanaka Y, Miyasaka T, Nagai A, Hirai K, Mano K, Miyashita H: The prolonged survival of human eosinophils with interleukin-5 and its inhibition by theophylline via apoptosis. Clin Exp Allergy 1996;26:10–15.

5 Momose T, Okubo Y, Horie S, Suzuki J, Isobe M, Sekiguchi M: Effects of intracellular cyclic AMP modulators on human cosinophil survival, degranulation and CD11b expression. Int Arch Allergy Immunol 1998;117:138–145.

6 Kita H, Abu-Ghazaleh RI, Gleich GJ, Abraham RT: Regulation of Ig-induced eosinophil degranulation by adenosine 3′,5′-cyclic monophosphate. J Immunol 1991;146:2712–2718.

7 Okubo Y, Hossain M, Horie S, Momose T, Suzuki J, Isobe M, Sekiguchi M: Inhibitory effects of theophylline and procaterol on eosinophil function. Intern Med 1997;36:276–282.
8 Tsukadaira A, Okubo Y, Horie S, Koyama S: Theophylline inhibits TNF-alpha-induced CD4 expression on human eosinophils and CD4+ eosinophil migration. Int Arch Allergy Immunol 2001;125:334–343.
9 Choo JH, Nagata M, Sutani A, Kikuchi I, Sakamoto Y: Theophylline attenuates the adhesion of eosinophils to endothelial cells. Int Arch Allergy Immunol 2003;131:40–45.
10 Nagata M: Differential effect of corticosteroids and theophylline on the adhesive interaction between eosinophils and endothelial cells. Allergol Int 2004;53:33–36.
11 Wenzel SE, Szefler SJ, Leung DYM, Sloan SI, Rex MD, Martin RJ: Bronchoscopic evaluation of severe asthma. Am J Resp Crit Care Med 1997;156:737–743.
12 Gibson PG, Simpson JL, Saltos N: Heterogeneity of airway inflammation in persistent asthma: evidence of neutrophilic inflammation and increased sputum interleukin-8. Chest 2001;119:1329–1336.
13 Wenzel SE, Schwartz LB, Langmack EL, Halliday JL, Trudeau JB, Gibbs RL, Chu HW: Evidence that severe asthma can be divided pathologically into two inflammatory subtypes with distinct physiologic and clinical characteristics. Am J Respir Crit Care Med 1999;160:1001–1008.
14 The ENFUMOSA Study Group: The ENFUMOSA cross-sectional European multicentre study of the clinical phenotype of chronic severe asthma. Eur Respir J 2003;22:470–477.
15 Kikuchi S, Nagata M, Kikuchi I, Hagiwara K, Kanazawa M: Association between neutrophilic and eosinophilic inflammation in patients with severe persistent asthma. Int Arch Allergy Immunol 2005;137(suppl 1):7–11.
16 Gibson PG, Simpson JL, Saltos N: Heterogeneity of airway inflammation in persistent asthma: evidence of neutrophilic inflammation and increased sputum interleukin-8. Chest 2001;119:1329–1336.
17 Kikuchi S, Kikuchi I, Kobayashi T, Hagiwara K, Kanazawa M, Nagata M: Eosinophil trans-basement migration induced by IL-8 and neutrophils. Am J Respir Cell Mol Biol 2006;34:760–765.
18 Nagata M, Sedgwick JB, Busse WW: Differential effects of granulocyte-macrophage colony-stimulating factor on eosinophil and neutrophil superoxide anion generation. J Immunol 1995;155:4948–4954.
19 Cassatella MA: The production of cytokines by polymorphonuclear neutrophils. Immunol Today 1995;16:21–26.
20 Henson PM, Wenzel SE: Neutrophils and their mediators in asthma; in Busse WW, Holgate ST (eds): Asthma and Rhinitis. Boston, Blackwell Scientific, 2000, pp 503–530.
21 Bradley JR, Johnson DR, Pober JS: Endothelial activation by hydrogen peroxide: selective increases of intercellular adhesion molecule-1 and major histocompatibility complex class I. Am J Pathol 1993:1598–1609.
22 Sellak H, Fanzine E, Hakims J, Pasquire C: Reactive oxygen species rapidly increase endothelial ICAM-1 ability to bind neutrophils without detectable upregulation. Blood 1994;83:2669–2677.
23 Siflinger-Birnboim A, Lum H, Del Vecchio PJ, Malik AB. Involvement of Ca^{2+} in the H_2O_2-induced increase in endothelial permeability. Am J Physiol 1996;270:L973–L978.
24 Fraticelli A, Serrano CV Jr, Bochner BS, Capogrossi MC, Zweier JL: Hydrogen peroxide and superoxide modulate leukocyte adhesion molecule expression and leukocyte endothelial adhesion. Biochem Biophys Acta 1996;1310:251–259.
25 Nagata M, Yamamoto H, Shibasaki M, Sakamoto Y, Matsuo H: Hydrogen peroxide augments eosinophil adhesion via β_2 integrin. Immunology 2000;101:412–418.
26 Cox G: Glucocorticoid treatment inhibits apoptosis in human neutrophils. Separation of survival and activation outcomes. J Immunol 1995;154:4719–4725.
27 Meagher LC, Cousin JM, Seckl JR, Haslett C: Opposing effects of glucocorticoids on the rate of apoptosis in neutrophils and eosinophilic granulocytes. J Immunol 1996;156:4422–4428.
28 Evans DJ, Taylor DA, Zetterstrom O, Chung KF, O'Connor BJ, Barnes PJ. A comparison of low-dose inhaled budesonide plus theophylline and high-dose inhaled budesonide for moderate asthma. N Engl J Med 1997;337:1412–1418.
29 Nassif EG, Weinberger M, Thompson R, Huntley W: The value of maintenance theophylline in steroid-dependent asthma. N Engl J Med 1981;304:71–75.

THE JOURNAL OF BIOLOGICAL CHEMISTRY VOL. 282, NO. 9, pp. 6532–6539, March 2, 2007

A Single Enzyme Catalyzes Both Platelet-activating Factor Production and Membrane Biogenesis of Inflammatory Cells

CLONING AND CHARACTERIZATION OF ACETYL-CoA:LYSO-PAF ACETYLTRANSFERASE[*][S]

Received for publication, October 13, 2006, and in revised form, December 1, 2006 Published, JBC Papers in Press, December 20, 2006, DOI 10.1074/jbc.M609641200

Hideo Shindou[‡1], **Daisuke Hishikawa**[‡], **Hiroki Nakanishi**[¶], **Takeshi Harayama**[‡], **Satoshi Ishii**[‡§1], **Ryo Taguchi**[¶‖], **and Takao Shimizu**[‡1,2]

From the [‡]*Department of Biochemistry and Molecular Biology, and* [¶]*Department of Metabolome, Faculty of Medicine, University of Tokyo, and* [§]*Precursory Research for Embryonic Science and Technology (PRESTO) and* [‖]*Core Research for Evolutional Science and Technology (CREST) of the Japan Science and Technology Agency, Hongo 7-3-1, Tokyo 113-0033, Japan*

Platelet-activating factor (PAF) is a potent proinflammatory lipid mediator eliciting a variety of cellular functions. Lipid mediators, including PAF are produced from membrane phospholipids by enzymatic cascades. Although a G protein-coupled PAF receptor and degradation enzymes have been cloned and characterized, the PAF biosynthetic enzyme, acetyl-CoA:lyso-PAF acetyltransferase, has not been identified. Here, we cloned lyso-PAF acetyltransferase, which is critical in stimulus-dependent formation of PAF. The enzyme is a 60-kDa microsomal protein with three putative membrane-spanning domains. The enzyme was induced by bacterial endotoxin (lipopolysaccharide), which was suppressed by dexamethasone treatment. Surprisingly, the enzyme catalyzed not only biosynthesis of PAF from lyso-PAF but also incorporation of arachidonoyl-CoA to produce PAF precursor membrane glycerophospholipids (lysophosphatidylcholine acyltransferase activity). Under resting conditions, the enzyme prefers arachidonoyl-CoA and contributes to membrane biogenesis. Upon acute inflammatory stimulation with lipopolysaccharide, the activated enzyme utilizes acetyl-CoA more efficiently and produces PAF. Thus, our findings provide a novel concept that a single enzyme catalyzes membrane biogenesis of inflammatory cells while producing a prophlogistic mediator in response to external stimuli.

Platelet-activating factor (PAF[3]; 1-*O*-alkyl-2-acetyl-*sn*-glycero-3-phosphocholine) is a phospholipid mediator that activates a G protein-coupled receptor (1–3) and results in pleiotropic and potent biological effects, including platelet activation, airway constriction, and hypotension (1). PAF is synthesized in various cells and tissues via two distinct pathways, the *de novo* and remodeling pathways (2, 4, 5), and the latter is regulated by extracellular signals and plays a critical role in stimulus-coupled PAF biosynthesis (2, 4–6). PAF synthesis induced by extracellular signals has been reported in murine peritoneal cells stimulated by calcium ionophore (7) or by PAF (8), in human eosinophils stimulated by fMet-Leu-Phe (9), in human neutrophils stimulated by acid stress (10), and in murine peritoneal macrophages stimulated by lipopolysaccharide (LPS) (11). In the remodeling pathway, the precursor of PAF, 1-*O*-alkyl-*sn*-glycero-3-phosphocholine (lyso-PAF), is synthesized from 1-*O*-alkyl-2-arachidonoyl-*sn*-glycero-3-phosphocholine (1-alkyl-phosphatidylcholine; PC) by the action of phospholipase A_2 (2, 4, 12, 13). Subsequently, lyso-PAF is converted to PAF by acetyl-CoA:lyso-PAF acetyltransferase (lyso-PAF acetyltransferase) (EC 2.3.1.67) (14). PAF is then rapidly degraded to lyso-PAF by PAF acetylhydrolases (15). Alternatively, lyso-PAF is again transformed into PC by the action of lysophosphatidylcholine (LPC) acyltransferase (2.3.1.23) (16).

A G protein-coupled PAF receptor was cloned in our laboratory (17), and PAF acetylhydrolases have been cloned and characterized by others (18, 19). Lyso-PAF acetyltransferase was initially demonstrated and partially characterized by Wykle *et al.* (14) in 1980. Since this first report, the enzyme activity has been detected in microsomes of rat spleen and lung as well as porcine leukocytes (14, 20). Although several groups have attempted to identify and characterize the enzyme from various sources (2, 4, 14, 21, 22), it has not yet been purified nor cDNA-cloned.

PC is a major component of cellular membranes and also plays an important role as a PAF precursor. PC is formed from diacylglycerol by a *de novo* pathway, originally described by Kennedy (23) in 1961 but is also generated from LPC by a remodeling pathway. Rapid turnover of the *sn*-2 acyl moiety of glycerophospholipids was described by Lands (Lands' cycle) (24–26) and is attributed to activation of phospholipases A_2 and lysophospholipid acyltransferases. Recently, we (27) and Chen *et al.* (28) independently cloned one of LPC acyltrans-

* This work was supported in part by Grants-in-Aid from the Ministry of Education, Science, Culture, Sports, and Technology of Japan (to T. S. and S. I.). The costs of publication of this article were defrayed in part by the payment of page charges. This article must therefore be hereby marked "*advertisement*" in accordance with 18 U.S.C. Section 1734 solely to indicate this fact.

The nucleotide sequence(s) reported in this paper has been submitted to the DDBJ/GenBank™/EBI Data Bank with accession number(s) AB244716 (mouse) and AB244718 (human).

[S] The on-line version of this article (available at http://www.jbc.org) contains supplemental Figs. 1 and 2.

[1] Supported by the Center for NanoBio Integration at the University of Tokyo.

[2] To whom correspondence should be addressed: Dept. of Biochemistry and Molecular Biology, Faculty of Medicine, University of Tokyo, 7-3-1 Hongo, Bunkyo-ku, Tokyo 113-0033, Japan. Tel.: 81-3-5802-2925; Fax: 81-3-3813-8732; E-mail: tshimizu@m.u-tokyo.ac.jp.

[3] The abbreviations used are: PAF, platelet-activating factor; LPS, lipopolysaccharide; PC, phosphatidylcholine; lyso-PAF acetyltransferase, acetyl-CoA:lyso-PAF acetyltransferase; LPC, lysophosphatidylcholine; DEX, dexamethasone; ER, endoplasmic reticulum; PAFR, PAF receptor; mLysoPAFAT and hLysoPAFAT, mouse and human LysoPAFAT, respectively; siRNA, small interfering RNA; $DiOC_6(3)$, 3,3′-dihexyloxacarbocyanine iodide.

Supplemental Material can be found at: http://www.jbc.org/cgi/content/full/M609641200/DC1

ferases designated LPCAT1, which is highly expressed in alveolar type II cells. Since PC synthesis occurs in a variety of different tissues, additional LPC acyltransferases may be present for membrane biogenesis.

Using the previously reported LPCAT1 (27) and an extensive genomic data base search as well as 5′- and 3′-RACE, we have identified a lyso-PAF acetyltransferase gene. The enzyme is primarily expressed in inflammatory cells and is induced by LPS. Surprisingly, the enzyme also catalyzes incorporation of arachidonoyl-CoA to produce PAF precursor membrane glycerophospholipids (LPC acyltransferase activity). Thus, we designated this enzyme LysoPAFAT/LPCAT2. Although this enzyme possesses both acetyltransferase and acyltransferase activity, only the acetyltransferase activity was enhanced by acute inflammatory signals. To our knowledge, this is the first documentation of a cDNA for LysoPAFAT/LPCAT2, a critically important enzyme in the biogenesis of PAF and in membrane homeostasis of inflammatory cells.

EXPERIMENTAL PROCEDURES

Materials—Various lysophospholipids and acyl-CoAs were obtained from Avanti Polar Lipids (Alabaster, AL). LPS from *Salmonella minnesota*, 4-amidinophenylmethanesulfonyl fluoride, dexamethasone (DEX), estradiol-17β, and linoleoyl-CoA (C18:2) were purchased from Sigma. [^{3}H]Acetyl-CoA (185 GBq/mmol) and [^{3}H]lyso-PAF (6.25 TBq/mmol) were obtained from Amersham Biosciences (Buckinghamshire, UK). [1-^{14}C]Arachidonoyl-CoA (2.22 GBq/mmol) was purchased from Moravec Biochemicals (Mercury Lane, CA). ODN1826 and poly(I:C) were purchased from InvivoGen (San Diego, CA).

Cloning of LysoPAFAT/LPCAT2—The mLysoPAFAT/LPCAT2 gene was identified based upon sequence similarity to the LPCAT1 gene (27) and LPA acyltransferase ζ gene (29) through a comprehensive basic local alignment search tool (BLAST) search. A 1.6-kb cDNA clone encoding the full-length mLysoPAFAT/LPCAT2 (DDBJ accession number AB244716) was cloned by PCR amplification using the forward primer 5′-CTAGCTAGCCACCATGGATTACAAGGATGACGATGACAAGAACCGATGCGCCGAGGCGGCCGC-3′, the reverse primer 5′-CCGCTCGAGTCAGTCCACCTTTTTGTCTGAGGTGCCCTC-3′, and a mouse spleen cDNA library as a template. The FLAG epitope (DYKDDDDK) was attached to the N terminus of mLysoPAFAT/LPCAT2 by PCR using a forward primer. Amplified PCR products were cloned into the pCXN2.1 vector, a slightly modified version of pCXN2 (30) with multiple cloning sites, and sequenced. Similarly, hLysoPAFAT/LPCAT2 cDNA (DDBJ accession number AB244718) was amplified by PCR and inserted into the pCXN2.1 vector.

Quantitative Real Time RT-PCR—Mouse total RNAs were prepared using the Absolutely RNA RT-PCR Miniprep Kit (Stratagene), and first strand cDNA was subsequently synthesized using Superscript II (Invitrogen). The PCRs were performed using FastStart DNA Master SYBR Green I (Roche Applied Science). The primers for mLysoPAFAT/LPCAT2 were designed to amplify a 167-bp fragment: forward primer, 5′-GTCCAGCAGACTACGATCAGTG-3′; reverse primer, 5′-CTTATTGGATGGGTCAGCTTTTC-3′. The primers for hLysoPAFAT/LPCAT2 were designed to amplify a 176-bp fragment: forward primer, 5′-TTGCTTCCAATTCGTGTCTTATT-3′; reverse primer, 5′-ATCCCATTGAAAAGAACATAGCA-3′.

Expression of FLAG-mLysoPAFAT/LPCAT2 in CHO-K1 Cells—After 48 h of transfection with FLAG-tagged enzyme using Lipofectamine 2000 (Invitrogen), cells in 10-cm dishes were scraped into 1 ml of ice-cold buffer containing 20 mM Tris-HCl (pH 7.4), 300 mM sucrose, and a proteinase inhibitor mixture, Complete (Roche Applied Science), and then sonicated three times on ice for 30 s. After centrifugation for 10 min at 800 × *g*, the supernatant was collected and centrifuged at 100,000 × *g* for 1 h. The resulting pellet was resuspended in buffer containing 20 mM Tris-HCl (pH 7.4), 300 mM sucrose, and 1 mM EDTA. Protein concentration was measured by the method of Bradford (31), using a commercially prepared protein assay solution (Bio-Rad) and bovine serum albumin (fraction V, fatty acid-free; Sigma) as a standard.

Confocal Microscopy—CHO-K1 cells were seeded onto 6-cm dishes before transfection. Six μg each of pCXN2.1 vector or FLAG-mLysoPAFAT/LPCAT2 were transfected using Lipofectamine 2000. 48 h post-transfection, vector- or FLAG-tagged enzyme-transfected cells were incubated with 2.5 μg/ml 3,3′-dihexyloxacarbocyanine iodide (DiOC$_6$(3)) (Invitrogen) and 10 μg/ml M5 anti-FLAG mouse monoclonal antibody (Sigma) in ¼× permeabilization buffer (Beckman Coulter, Marseille, France). After washing, cells were incubated with 10 μg/ml Alexa Fluor 546 goat anti-mouse IgG (Eugene, OR) for 30 min. Confocal microscopy was performed with an LSM510 laser-scanning microscope (Carl Zeiss) equipped with a ×63 water immersion objective lens (numerical aperture = 1.2). FLAG-mLysoPAFAT/LPCAT2 was monitored by excitation at 543 nm with a helium/neon laser and by emission with a 585-nm long path filter. For the detection of DiOC$_6$(3), the excitation was at 488 nm with an argon laser, and emissions were taken with a 505–550-nm band pass filter.

Assay of Lyso-PAF Acetyltransferase—The lyso-PAF acetyltransferase activity was determined according to the method of Kume *et al.* (20), except for washing resin one time before and eight times after application of the reaction mixture. Briefly, 100 μM [^{3}H]acetyl-CoA (1.11 GBq/mmol) and protein were incubated at 37 °C for 10 min in the presence or absence of 20 μM lyso-PAF (Cayman). Subsequently, the product was bound to C8 resin (Millipore), washed, and eluted. The difference between the radioactivities obtained in the presence and absence of lyso-PAF corresponded to lyso-PAF acetyltransferase activity.

Assay of Lysophospholipid Acetyltransferase and Acyltransferase by TLC—The acyltransferase activity was measured in two ways: (i) conversion of [1-^{14}C]lyso-PAF (293 MBq/mmol) to PC in the presence of acetyl- and acyl-CoA and (ii) the transfer of [^{3}H]acetyl-CoA (1.11 GBq/mmol)- or [^{14}C]arachidonoyl-CoA (1.11–2.035 GBq/mmol) to lysophospholipids to form phospholipids. The reaction mixture contained 20 mM Tris-HCl (pH 7.4), 2 mM $CaCl_2$, 1 mg/ml PC, 5 mM 2-mercaptoethanol, 20 μM 4-amidinophenylmethanesulfonyl fluoride (Sigma), a proteinase inhibitor mixture, 10 or 100 μM acyl-CoA, 20 μM lysophospholipid, and enzyme in a total volume of 100